2.1. Introduction

Mario Betti (1875–1942), a very active distinguished Italian chemist, [1] started his work in Schiff's laboratory at the University of Florence. From the Schiff's laboratory he moved to the University of Cagliari followed by Siena, Genoa and finally Bologna, where he worked as the successor of Giacomo Ciamician. His main research interests in stereochemistry were directed towards

a) Resolution of racemic compounds
b) Relationship between molecular constitution and optical rotator power
c) Asymmetric synthesis with the aid of chiral auxiliaries or in the presence of circularly polarised light.

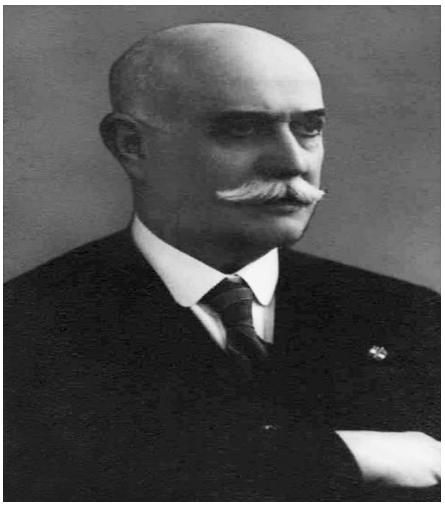

Mario Betti, the person behind Betti reaction (1875-1942)

2.1.1. The Betti reaction

The reaction between ammonia or amine with formaldehyde yield imine which on reaction with enolisable carbonyl compounds resulted in formation of amino alkyl compounds. This procedure was first performed by the German scientist, Carl Ulrich Franz Mannich in 1912 and the reaction is known as Mannich aminoalkylation.

In 1900, Betti hypothesized, and later proved that 2-naphthol should be a good carbon nucleophile towards the imine produced from benzaldehyde and aniline as shown in Scheme 2.1.

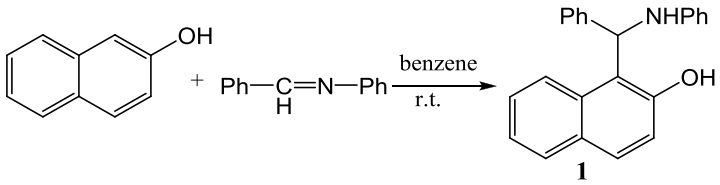

Scheme 2.1 Reaction between 2-naphthol and an imine.

Later, [2] Betti isolated the product and reported that the product i.e. imine derivative **2a** can be obtained from three component condensation of 2-naphthol, an ethanolic solution of ammonia and two equivalent of benzaldehyde (Scheme 2.2). Smith et al. [3] later proved that the imine product remain in equilibrium with its oxazoline **2b** form.

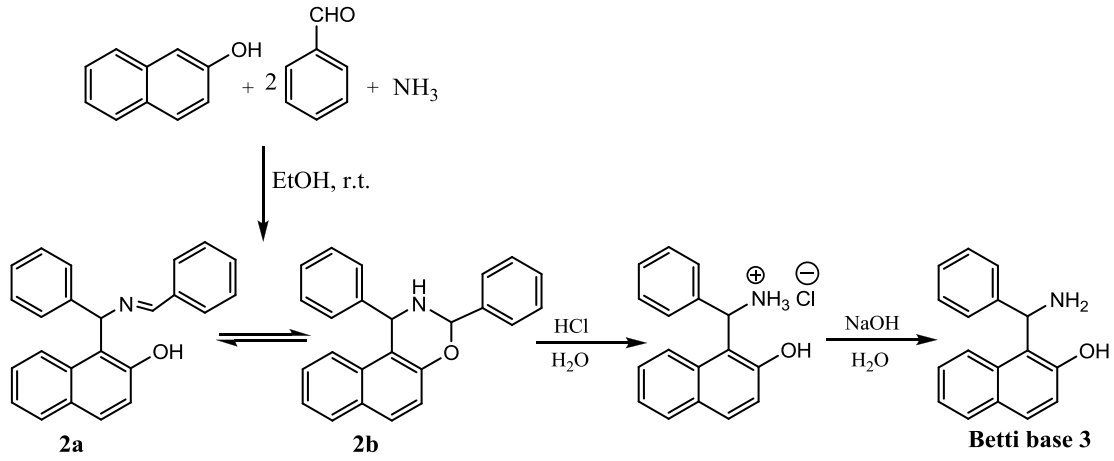

Scheme 2.2 The Betti reaction

The hydrochloride salt of intermediate **2** on treatment with saturated solution of sodium carbonate yielded Betti base **3** which was successfully resolved into two optical isomers using tartaric acid through classical resolution method. [4]

In 1998, Naso et al. [5] determined absolute configuration of the hydrobromide salt of Betti base by an X-ray experiment. (Fig. 2.1)

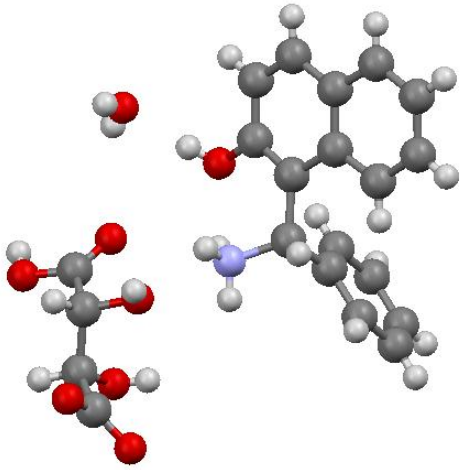

Figure 2.1 Crystal structure of *S*-Betti base hydrobromide

Naso et al. [5] have reported an improved procedure for separation of enantiomers of Betti base using a mixture of ethanol and methanol.

A very simple, easily scalable separation of the enantiomers of Betti base through kinetic resolution has been reported by Hu et al. [6] using L-(+)-tartaric acid, in acetone. (Scheme 2.3)

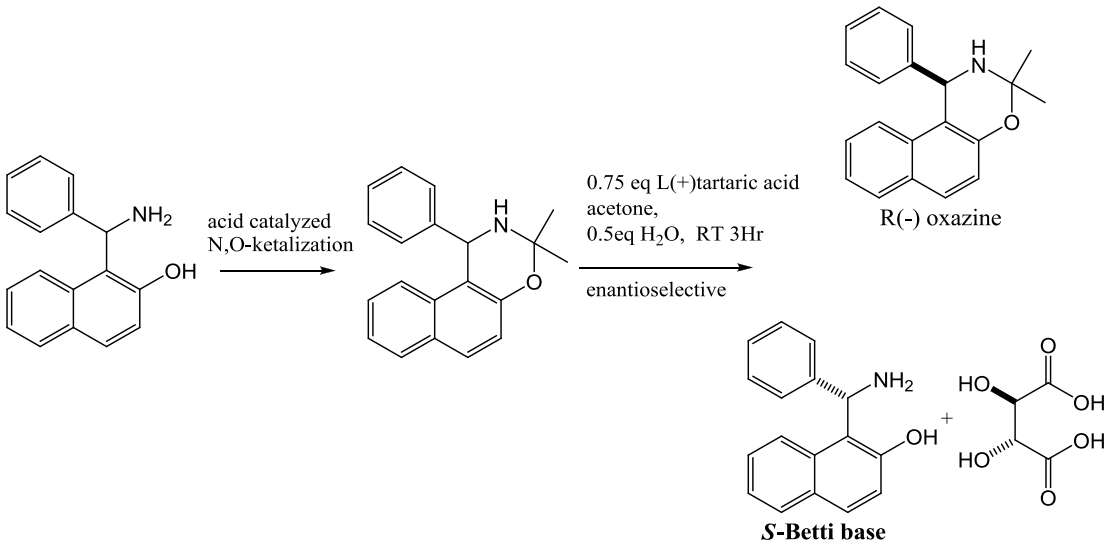

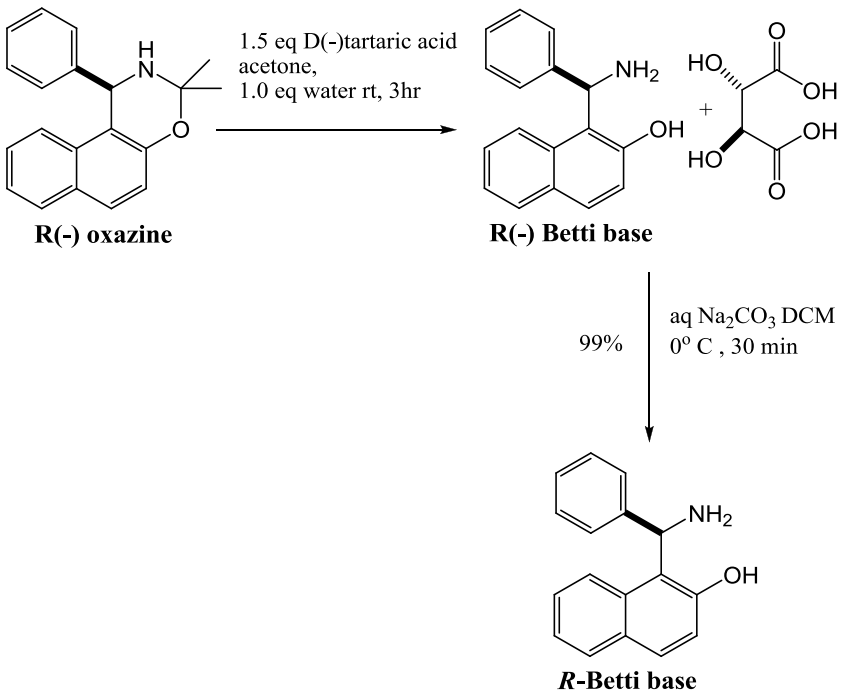

Scheme 2.3 Resolution of Betti base into its enantiomers

Alfonsov et al. [7] has reported a one-pot methodology to separate the enantiomers of Betti base, starting from the imine/oxazine precursor using tartaric acid in DCM/methanol.

2.1.1.1. Derivatives of Betti base

The Betti reaction could be used to synthesize more complex molecular structures by assembling three simple components namely 2-naphthol, aryl aldehydes and ammonia, or amines.

Littman and Brode [8] have synthesized different derivatives of Betti base using different amines like dimethylamine and piperidine instead of ammonia. (Scheme 2.4)

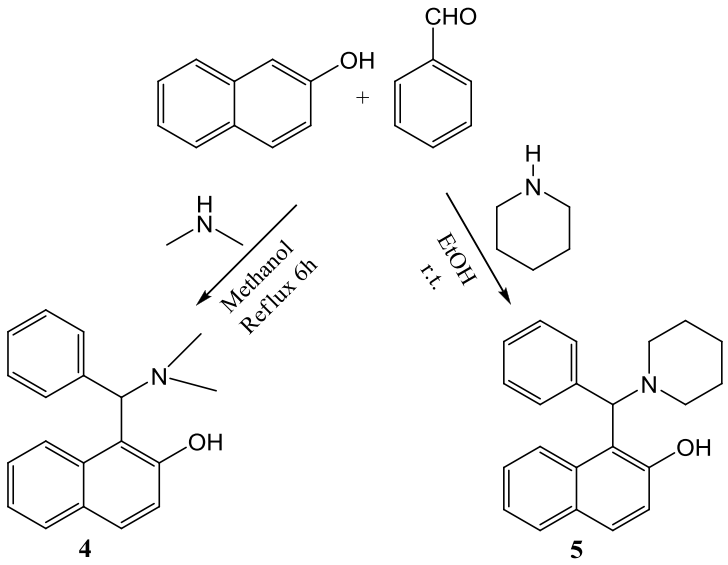

Scheme 2.4 The Betti reaction with dimethylamine and piperidine

An optically active camphorsulphonic acid was used for resolution of these compounds.

According to Littman and Brode secondary amines would react with benzaldehyde via formation of a benzylidinediamine intermediate. This intermediate attacks 2-naphthol yielding aminobenzylnaphthol, after elimination of the amine as shown in Scheme 2.5

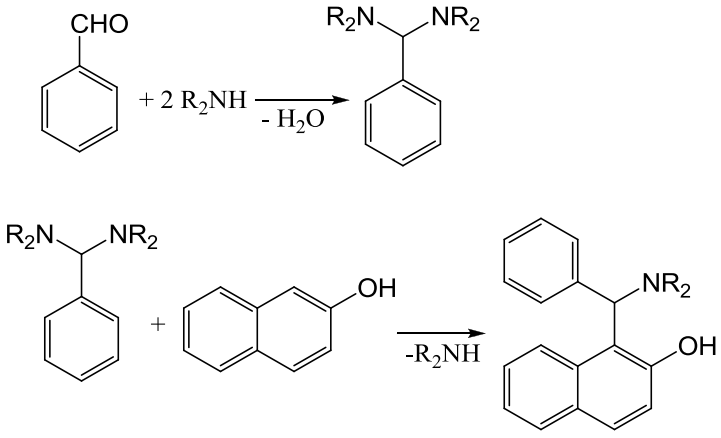

Scheme 2.5 The Betti reaction with secondary amines

However, alternative mechanism based upon the reaction between amine and an adduct formed between 2- naphthol and benzaldehyde cannot be ruled out. (Scheme 2.6)

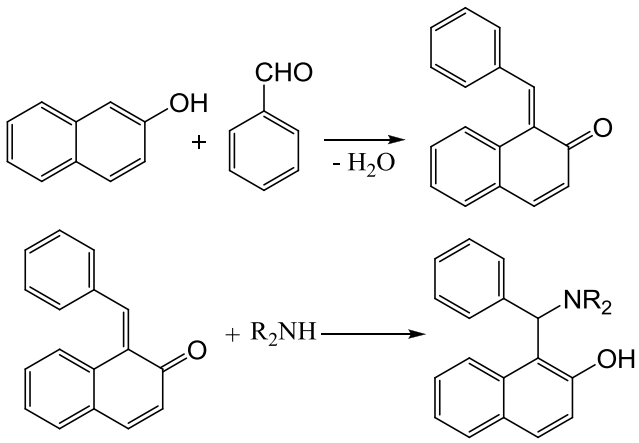

Scheme 2.6 A different sequence for the Betti reaction

Periasamy et al. [9] have synthesized 1-(α-pyrrolidinyl benzyl)-2-napthol (Scheme 2.7) using pyrollidine as amine and resolved by tartaric acid (Scheme 2.8).

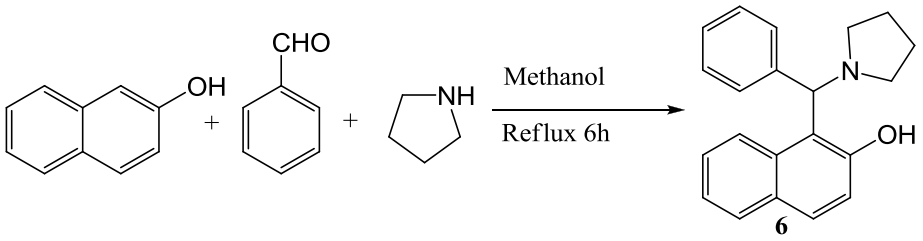

Scheme 2.7 Betti reaction with pyrrolidine

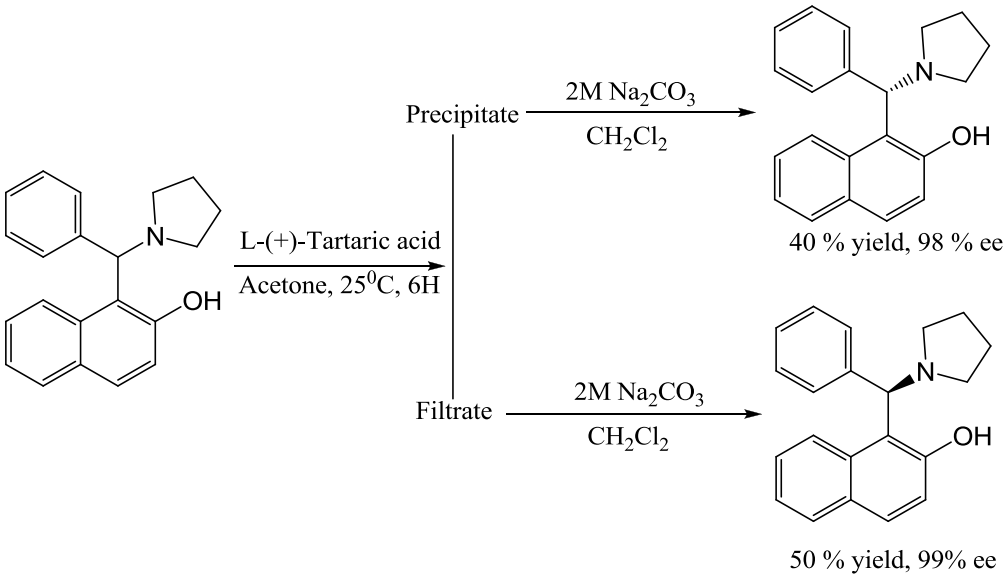

Scheme 2.8 Resolution of 1-(α-pyrrolidinyl benzyl)-2-naphthol

Several bases have been synthesized by the Betti reaction with different aldehydes by Fulop et al. [10-12] (Scheme 2.9)

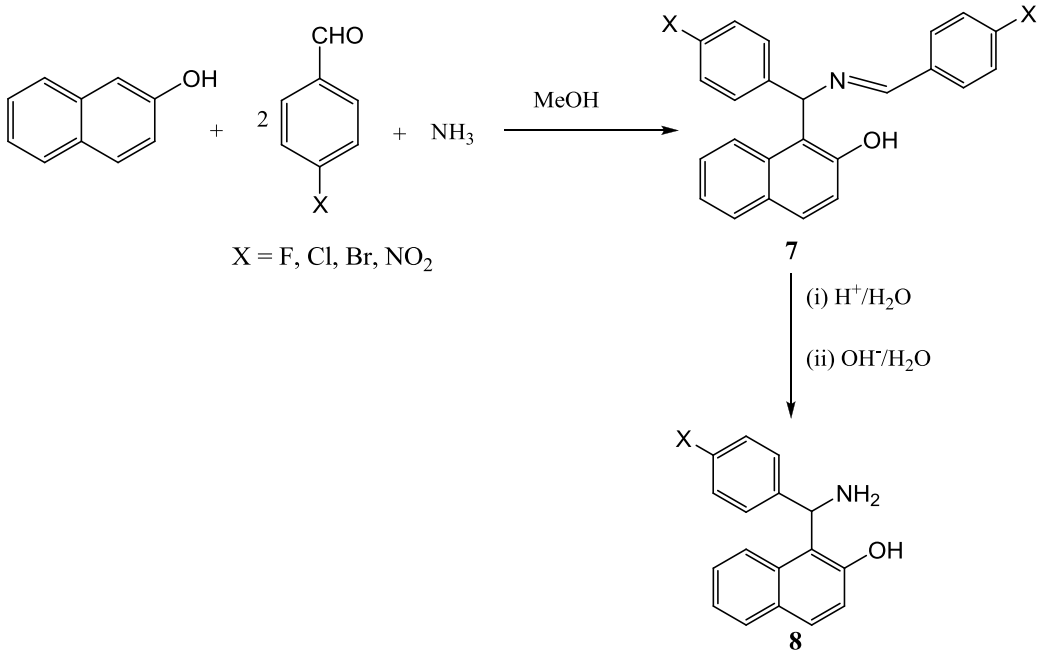

Scheme 2.9 Synthesis of new Betti bases

Xiong [13] have reported synthesis of bis Betti bases, **9** (Scheme 2.10) by reaction of 1 equiv of 2,6-dihydroxynaphthalene with 2 equiv of piperidine or morpholine and cyanobenzaldehyde at 100 °C .

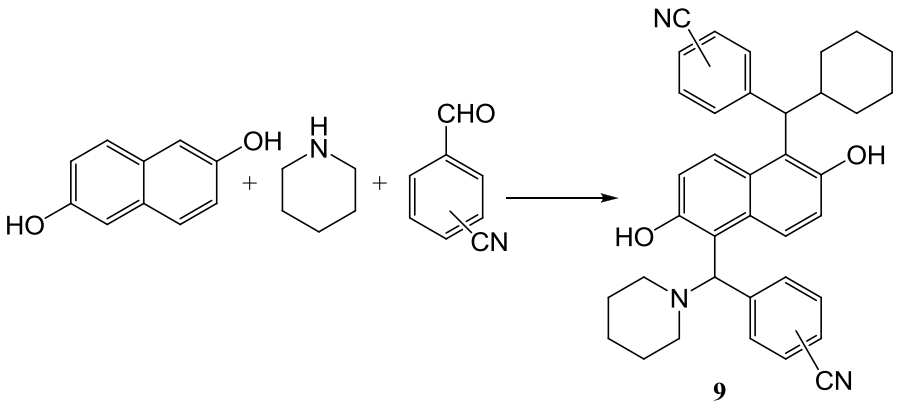

Scheme 2.10 Synthesis of bis Betti base using 2,6- dinaphthols

Synthesis of 1-naphtholyl tetrahydroisoquinolines **10** have been reported by Li et al.[14]

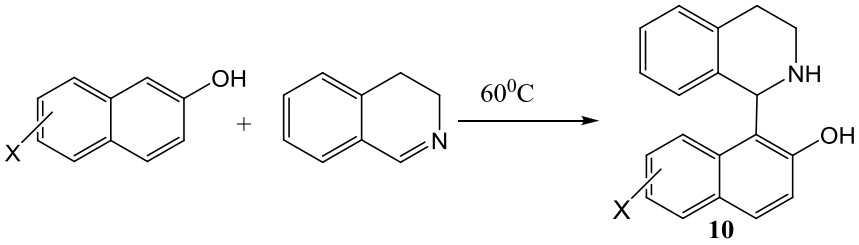

10

X = H, 6-MeO, 7-MeO, 6-PhCO, 6-Br

Scheme 2.11 Betti reaction with 3,4-dihydroisoquinoline

A new era in the field of synthesis of Betti Base began when the Betti reaction was performed by Palmieri et al. [15-17] with enantiopure amines. In this approach, the presence of a resolved stereogenic centre on the amine, induced formation of a new stereogenic centre with high stereoselectivity. Following this procedure, after a simple crystallisation, a desired aminobenzylnaphthol with two fully resolved stereogenic centers was achieved.

A solvent free Betti reaction of 2-naphthol, aryl aldehydes and (*R*)-1-phenylethylamine or (*R*)-1-(1-naphthyl) ethylamine yielded different substituted Betti bases. [15,17]

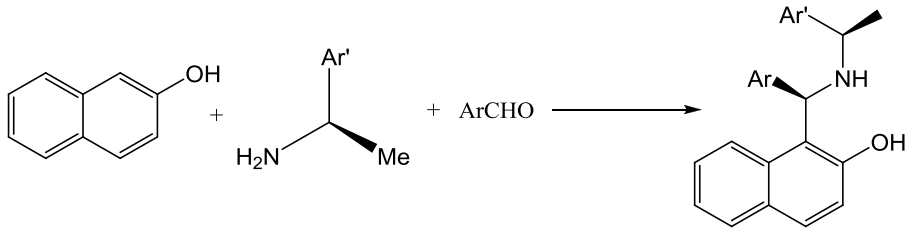

(*R*,*R*) 11

Scheme 2.12 Betti reaction with (*R*)-1-arylethylamine

Aminobenzylnaphthol **12** was prepared by a different synthetic route, [18] represented by the reaction between commercially available (*S*)-(–)-N-α– dimethylbenzylamine, benzaldehyde, and 2-naphthol without any solvent. The same solvent-free procedure was used in the reaction of (*S*)-N-α-dimethylbenzylamine with 1-naphthaldehyde and 2-naphthol at 85 °C [19]

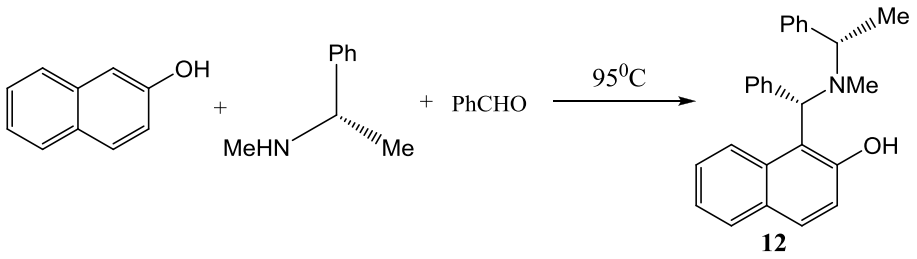

Scheme 2.13 Betti reaction with (*S*)-(–)-N-α-dimethylbenzylamine

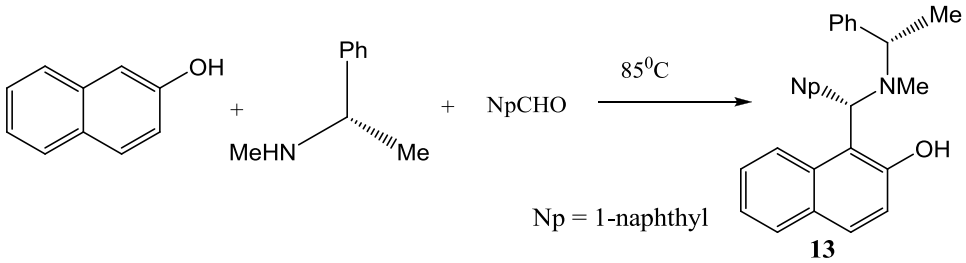

Scheme 2.14 Betti reaction with 1-naphthaldehyde and (*S*)-N, α-dimethylbenzylamine

Palmieri et al. [15-17] have synthesized aminonaphthols with chiral aldehydes as well wherein the solvent free reaction was carried out by mixing 2-naphthol with primary or secondary amines and chiral aldehydes at room temperature.

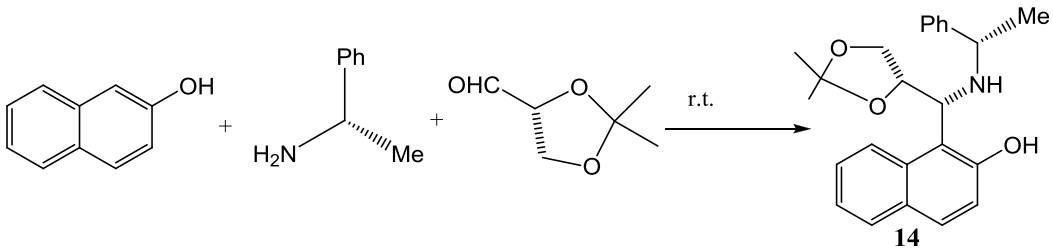

Scheme 2.15 Betti reaction with chiral non-racemic aldehydes and amines

2.1.1.2. New synthetic route for the synthesis of Betti base

Ammonium carbamate or ammonium hydrogen carbonate under microwave irradiation was proposed as an alternative and convenient source of ammonia, for the synthesis of Betti base. [20] Ghandi et al. [21] have quantitatively synthesized Betti base in aqueous medium. Atul kumar et al. [22] have developed an efficient non-ionic surfactant, Triton X-100 catalyzed multicomponent Mannich-type reactions for the synthesis of Betti base from aldehydes, secondary amines, and 2-naphthol in water.

Triton X-100 forms stable colloidal medium which plays an essential role in acceleration of the reactions in water.

2.1.2. Electrochemical study of amino phenols

Electrochemical behavior of phenol and particularly with a pendant amine has attracted much attention in the last decade, because of its involvement in the biologically important processes. [23-40] The survey of literature revealed publication of a large volume of studies on model systems to understand mechanism of formation of phenoxyl radical. Among these the electrochemical behavior of ortho substituted 4,6-di(tert butyl) phenols with phenolic hydrogen atom H-bonded to the N-atom of the nearby amine have been extensively studied by Yoshihiro Matsumura et al. Jean Michel Saveant et al. and James M. Mayer et al. [23-40]

Betti Base with similar structure i.e. with sp^3 hybridized carbon attached to phenyl ring, amine and naphthol, is expected to exhibit an interesting redox property. This observation calls for an exhaustive investigation of the redox property of the ligand.

Molecular electrochemistry, through nondestructive techniques such as CV, has been proved to be very useful in characterizing electron transfers and deciphering mechanisms in which chemical reactions are associated with electron transfer.

Hence in the present work, the electrochemical behavior of the ligands was studied by CV.

2.1.2.1. Cyclic voltammetry

Cyclic voltammetry (CV) is one of the most used techniques to study the electrochemical behavior of organic compounds. It is an excellent technique to probe chemical changes that occur as a result of electron transfer and is critical for understanding the reactivity and electronic structure of redox-active ligands. Often electrochemistry allows for transient species to be generated and observed that would otherwise be unobtainable. One of the strengths of the CV technique is in the identification of electrochemical reactions involving combination of electron transfer and chemical reaction steps through proper analysis of CV curves recorded at various scan rates.

The main components of a Cyclic Voltammeter are the Reference electrode, Auxillary electrode, Working electrode and a Potentiostat (Fig. 2.2).

Figure 2.2 Image of Potentiostat with Electrochemical cell

The Potentiostat is an instrument that controls the potential of the working electrode with respect to the reference electrode while measuring the current flow between the working electrode and counter electrode. In CV, the potential of a working electrode is cycled linearly between two potential values at which the oxidation and reduction of a solute occurs. The resulting current-potential curve is called a cyclic voltammogram.

2.2. Experimental

2.2.1. Materials

Benzaldehyde, β- naphthol, pyrrolidine, dimethyl amine, anisaldehyde, L(+)/R(–) Tartaric acid were purchased from Fisher Scientific. Freshly distilled solvents were employed for all synthetic purposes. Spectroscopic grade solvents were employed for spectral work. All other chemicals used were of AR grade.

2.2.2. Synthesis of Betti base and its derivatives

2.2.2.1. Synthesis of 1-(α-amino benzyl)-2-napthol (BB/L_1)

1-(α-amino benzyl)-2-napthol commonly known as Betti base (BB/L_1) and its derivative 1-(α-amino-p-methoxybenzyl)-2-napthol (ABB/L_8) were synthesized and resolved by reported methods [2-5]. In a 250 mL round-bottomed flask was placed a cold solution of 36 g. (0.25 mole) of β-naphthol in 50 mL of methanol. To this solution, 53 g. (0.50 moles) of freshly distilled benzaldehyde/anisaldehyde followed by 50 mL of methanol saturated with ammonia were added. The solution turned red. The stopper of the flask was removed after two hours, allowing the excess ammonia to escape. After about twelve hours, the condensation product, separated as white needles, was filtered with suction and washed with 50 mL of methanol. An additional quantity of the condensation product was obtained from the mother liquors on standing for three days. The yield of the condensed product was 80-90 per cent and its melting point was found to be 148–150°C.

The condensation product obtained was introduced into a 500-mL round-bottom flask attached to a steam distillation assembly and treated three times its volume with 20 per cent hydrochloric acid. The mixture was steam distilled to remove all benzaldehyde formed by the hydrolysis (about two hours). The mixture in the flask was cooled thoroughly and filtered with suction. The yield of about 70-80 per cent with 190–220°C melting point was obtained.

In order to obtain amine, the finely divided hydrochloride salt was placed in a 500 mL beaker and stirred to a smooth paste with 100 mL of water. To this was added 50 g. of crushed ice, and the mixture was cooled in an ice bath. 200 mL of saturated solution of Na_2CO_3 was added slowly with stirring until a nearly clear solution resulted. The cold solution was transferred to a separatory funnel and extracted with 100 mL of DCM. The combined organic extracts were dried overnight over 50 g. of anhydrous sodium sulfate, filtered, and evaporated to obtain the amine product. The total yield of the product was 73–75 per cent which melted at 124–125°.

2.2.2.2. Kinetic Resolution of BB (L_1)

To a stirred suspension of (±-3•HCl) (5.0 g, 17.5 mmol) in acetone (45 mL) was added Et_3N (1.8 g, 17.5 mmol) at 0 °C. Twenty minutes later, H_2SO_4 (98%, 0.1 mL) was added. The resultant mixture was stirred at room temperature for 1 h (monitored by TLC), and saturated aqueous solution of Na_2CO_3 (10 mL) was added. After most acetone was removed by rotavapor, the residue was diluted with CH_2Cl_2 (45 mL) and H_2O (45 mL). The separated aqueous layer was extracted with CH_2Cl_2, and the combined organic layers were washed with H_2O and brine and dried over Na_2SO_4. Removal of the solvent gave crude product, which was purified by recrystallization (EtOAc) to give (±)-oxazine derivative (4.8 g, 96%) as colorless crystals which melted at 124-126 °C

To a stirred solution of **(±)**-oxazine (4.8 g, 16.6 mmol) in acetone (30 mL) was sequentially added a solution of L-(+)-tartaric acid (1.9 g, 12.7 mmol) in acetone (40 mL) and H_2O (0.02 mL). After the resultant mixture was stirred at room temperature for 3 h, the white solid was collected by filtration and was washed with acetone (2×25 mL) to give (*S*)-3•tartaric acid salt (3.2 g, 48%) which melted at 186-188°C. To the filtrate was added a saturated aqueous solution of Na_2CO_3 (10 mL). After most of the acetone was removed by rotavapor, the residue was diluted with CH_2Cl_2 (40 mL) and H_2O (20 mL). The separated aqueous layer was extracted with CH_2Cl_2, and the combined organic layers were washed with H_2O and brine and dried over Na_2SO_4. Removal of the solvent gave crude product, which was purified by recrystallization (EtOAc) to give (*R*)-Oxazine (1.6 g, 47%) as colorless crystals which melted at 148-150°C.

The (*R*)-oxazine was similarly treated with D-(–)-tartaric acid to form (*R*)-3•tartaric acid salt.

Preparation of (S)-(+) / (R)-(–) Betti base

To a stirred suspension of (*S*)-3/ (R)-3•tartaric acid salt (5.0 g, 12.5 mmol) in CH_2Cl_2 (30 mL) was added an aqueous solution of Na_2CO_3 (10%, 30 mL) at 0°C. The resultant mixture was stirred until the solid disappeared completely (30 min). The separated aqueous layer was extracted with CH_2Cl_2 and the combined organic layers

were washed with H_2O and brine and dried over Na_2SO_4. Removal of the solvent gave (S)-(+) / (R)-(–) Betti base as colorless crystals; mp 133-134 °C.

2.2.2.3. Synthesis of 1-(α-pyrrolidinyl benzyl)-2-napthol

1-(α-pyrrolidinyl benzyl)-2-napthol (PBB/**L_4**) was synthesized and resolved by reported methods. [9] In a 250 mL round bottomed flask was placed a solution of 2-naphthol (14.4 g, 100 mmol) in 50mL of Methanol. To this Benzaldehyde (13.2 mL, 130 mmol) followed by pyrrolidine (8.4 mL, 100 mmol) was added and the reaction mixture was refluxed for 6 h and brought to room temperature. The precipitate was filtered and washed with Methanol to isolate 1-(α-pyrrolidinylbenzyl)-2-naphthol as white solid which melted at 176–177°C.

2.2.2.4. Resolution of PBB/L_4

The L-(+)-tartaric acid (0.75 g, 5 mmol) and **L_4** (1.5 g, 5 mmol) were taken in acetone (70mL) and the contents were stirred at 25°C for 6 h and filtered. The precipitate was suspended in a mixture of CH_2Cl_2 and aq Na_2CO_3 (2M) and stirred until dissolution occurred. The organic extracts were washed with brine, dried (Na_2SO_4) and evaporated to obtain the enantiomer (*S*)-(+)-L_4 (40% yield). The filtrate was concentrated to get crude product. The crude product was then treated with anhydrous oxalic acid in acetone (70 mL). The reaction was stirred for 6 h to get (R)-(–)-L_4•oxalic acid salt. The salt was treated as outlined above to obtain the enantiomer (R)-(–)-L_4 (55% yield).

2.2.2.5. Synthesis of 1-(α-dimethylamino benzyl)-2-napthol and its derivative

1-(α-dimethylamino benzyl)-2-napthol (DBB/L_7) and its derivative 1-(α-dimethylamino-p-methoxybenzyl)-2-napthol (ADBB/L_9) were synthesized by reported methods. [5] In a 250 mL round bottomed flask was placed a solution of 2-naphthol (14.4 g, 100 mmol) in 50mL of Methanol. To this Benzaldehyde / anisaldehyde (130 mmol) followed by dimethylamine (10.1 g, 100 mmol) was added and the reaction mixture was refluxed for 6 h and brought to room temperature. The precipitate was filtered and washed with Methanol to isolate **L_7** and **L_9** as white solid which melted at 165 & 168°C respectively.

2.3. Characterization of Betti base and its derivatives

Betti base and its derivatives were characterized by, ^{1}H NMR, ^{13}C NMR and CD. The NMR spectra were collected on a 400 MHz spectrometer (Bruker AV 400) in $CDCl_3$ and d_6-DMSO. The SOR of the ligands L_2, L_3, L_5 & L_6 (c = 1.0, $CHCl_3$) were measured on a Jasco P-2000 Polarimeter. The CD spectra of 0.5 mM solution of the optically pure ligands (**L_2,L_3,L_5,L_6**) in chloroform were recorded using a Jasco J-810 Spectro-polarimeter in the range 250–800 nm.

2.3.1. Electrochemical analysis

Cyclic voltammetric studies of Betti bases (1.0 mM in DCM) using $TBAPF_6$ as supporting electrolyte were performed on a CH Instruments 600C potentiostat, with a glassy carbon as working electrode (area 0.071 cm^2), Ag/Ag^+ reference electrode (0.01 M $AgNO_3$ in acetonitrile) and Pt wire as a counter electrode. To obtain reproducible results, the glassy carbon electrode was polished using polishing kit (CHI120) which consisted of a polishing polyurethane pad, alpha Al_2O_3 (particle size 1.0 & 0.3 μm) and gamma Al_2O_3 powder (particle size 0.05 μm). The electrode was polished with 0.05 μm alumina, sonicated (ultrasound bath) for 3 min and finally rinsed with deionized water before each measurement. Solutions were deoxygenated by bubbling dry nitrogen prior to the potential sweep. All experiments were carried out at room temperature.

2.4. Results and Discussion

2.4.1. Verification of the synthesized compounds

The purity of the compounds has been checked by TLC and further confirmed by NMR spectral analysis. The data for the ^{1}H NMR and ^{13}C NMR are given below. (SI; Fig. 2.2 –2.7)

BB

^{1}H NMR($CDCl_3$): δ = 7.67-7.70 (m, 3H), 7.13-7.42 (m, 8H), 6.10 (s, 1H), 2.39 (br. S, 2H)

^{13}C NMR($CDCl_3$): δ 156.9, 142.4, 132.0, 129.7, 129.0, 128.7(2C), 128.5, 127.9, 127.3(2C), 126.4, 122.4, 121.2, 120.5, 115.1, 55.9.

The absence of peaks at δ = 156.9, 142.4, 132.0 & 115.1 in DEPT-90 and DEPT-135 indicates the presence of four tertiary carbons in Betti base.

PBB

^{1}H NMR($CDCl_3$): δ = 13.8 (br s, 1H), 7.88-7.65 (m, 4H), 7.64-7.21 (m,6H), 5.12 (s, 1H), 3.27(br s 1H), 2.60-2.27(br s, 3H), 1.85(br s, 4H).

DBB

^{1}H NMR($CDCl_3$): δ = 13.8 (br s, 1H), 7.86-7.56 (m, 5H), 7.36-7.15 (m,6H), 4.98 (s, 1H), 2.39-2.33(br s, 6H).

ABB

^{1}H NMR($CDCl_3$): δ = 7.72-7.67 (m, 3H), 7.39-7.14 (m, 5H), 6.84-6.81 (m,2H), 6.10 (m, 1H), 3.72 (s, 3H).

ADBB

^{1}H NMR($CDCl_3$): δ = 13.8 (br s, 1H), 7.67-7.46 (m, 5H), 7.37-7.14 (m,3H), 6.78-6.76 (m, 2H), 4.91 (s, 1H), 3.70 (s, 3H), 2.39-2.32(br s, 6H).

Based on NMR data the structures of the synthesized compounds confirmed and are as follows:

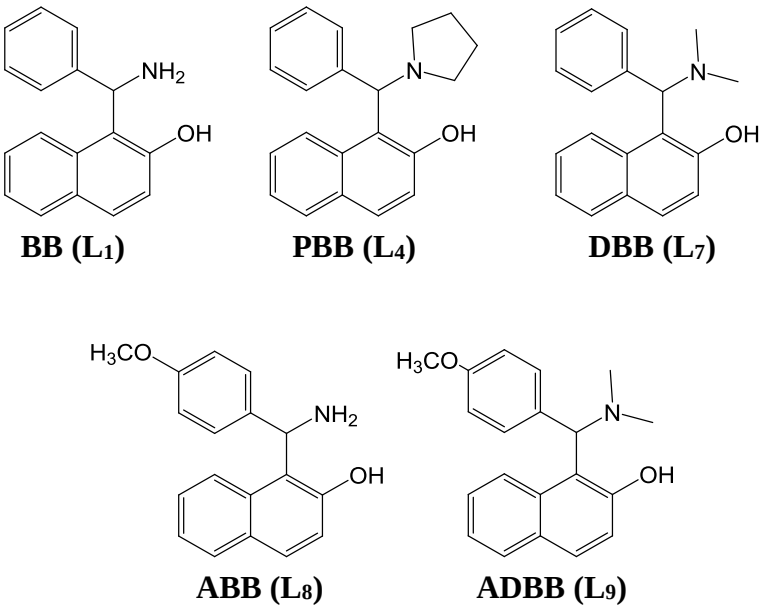

BB (L_1) **PBB (L_4)** **DBB (L_7)**

ABB (L_8) **ADBB (L_9)**

Figure 2.3 Structure of Betti base and its derivatives

2.4.2. Circular Dichroism (CD) Spectroscopic analysis

The ligands **L_1** and **L_4** had been resolved to their optically pure form by reported method. [6] The efforts for the resolution of ligands **L_7**, **L_8** and **L_9** were unsuccessful. The CD spectra of enantiomeric pairs **L_2** & **L_3** and **L_5** & **L_6** bear mirror image relationship (Fig. 2.4), as expected. The *S*- ligands (**L_2** & **L_5**) exhibit positive Cotton effects for intraligand electronic transitions at 290 nm and 340 nm, where as the *R*-ligands (**L_3** & **L_6**) exhibit negative Cotton effects for intraligand electronic transitions at 290 nm and 340 nm.

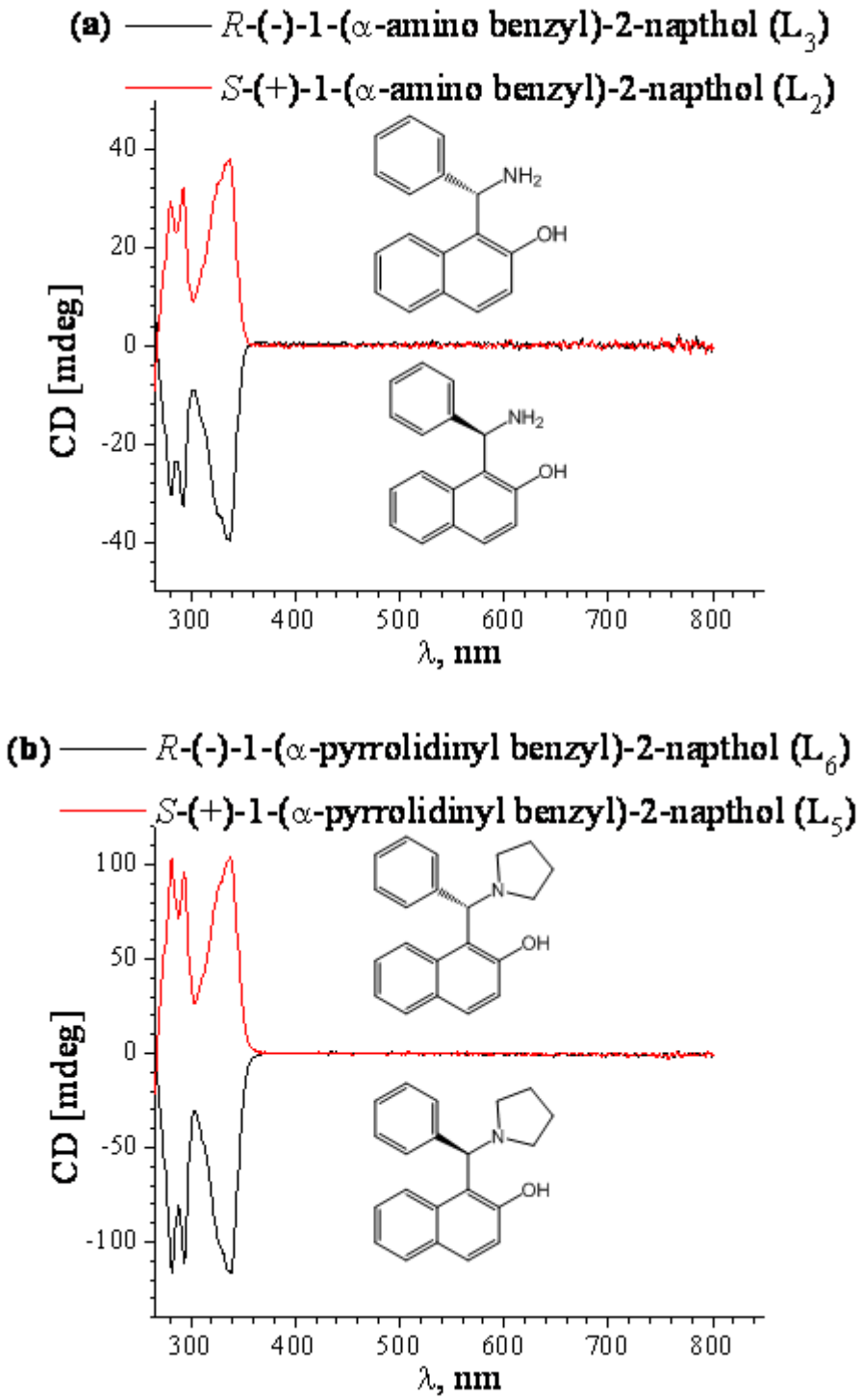

Figure 2.4 Circular Dichroism spectra (0.5mM) in 10mL of chloroform. (a) CD spectra of **L2** and **L3** (b) CD spectra of **L5** and **L6**

2.4.3. Cyclic voltammetric study of Ligands

The cyclic voltammograms of ligands **L_1**, **L_4**, **L_7**, **L_8** and **L_9** (1.0 mM , 100 mV/sec) in the potential window of -0.9 V to 1.2 V are given in Figure 2.5.

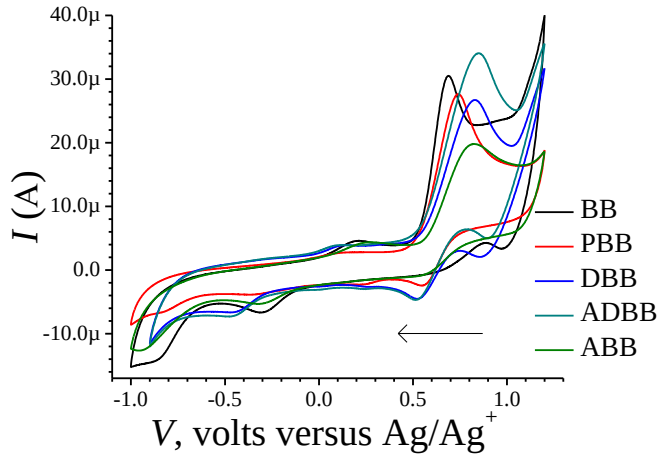

Figure 2.5 Cyclic voltammograms of Betti bases (1mM in DCM) using 0.1 M $TBAPF_6$ as the supporting electrolyte.

The redox potentials of the Betti bases are tabulated in the Table 2.1.

Table 2.1 Electrochemical data[a] for ligands at at 25 ± 2 °C in DCM solution.

Name of Ligand	Reduction Potential (Volt)		Oxidation Potential (Volt)	
	c1	c2	a1	a2
BB (L_1)	–0.31	–0.87	0.69	0.20
PBB (L_4)	0.55	–0.36	0.74	0.13
DBB (L_7)	0.52	–0.48	0.82	0.14
ABB (L_8)	–0.32	–0.95	0.82	0.27
ADBB (L_9)	0.52	–0.47	0.85	0.10

[a] Potential measured vs. Ag/Ag^+ reference electrode; scan rate $100mVs^{-1}$; supporting electrolyte : $TBAPF_6$ (0.1M); ligand concentration : 0.001M.

As can be seen from the Table 2.1, significant difference in the reduction potential of **L_1**, **L_4** and **L_7** is observed. These are positive for **L_4** and **L_7** where as negative for **L_1**.This is attributed to the substituted tertiary amine and lack of H-bond formation between phenol radical formed after oxidation and tertiary amine in contrast the Betti

base **L_1** containing primary amine. A similar observation has been made by Matsumura et al. and Thomas et al. [23]

It is also observed that substitution of methoxy group para to the benzyl ring has no major effect on the redox behavior of the ligand **L_8** and **L_9**. This is probably due to the position of the methoxy group which being away from the redox active centers of the molecule does not affect the redox potentials.

2.4.3.1. Cyclic voltammetric study of Betti base (L_1)

To understand the redox process thoroughly, a detailed study of ligand **L_1** has been carried out. The cyclic voltammograms of Betti base (1.0 mM , 100 mV/sec) in the potential window of (a) 0.5 V to -0.9 V, (b) 1.2 V to -0.9 V and (c) 0.0 V to -0.9 V followed by reverse scan from -0.9 V to 1.2 V and finally second cycle from 1.2 V to -0.9 V are shown in Figure 2.6. (a),(b),(c).

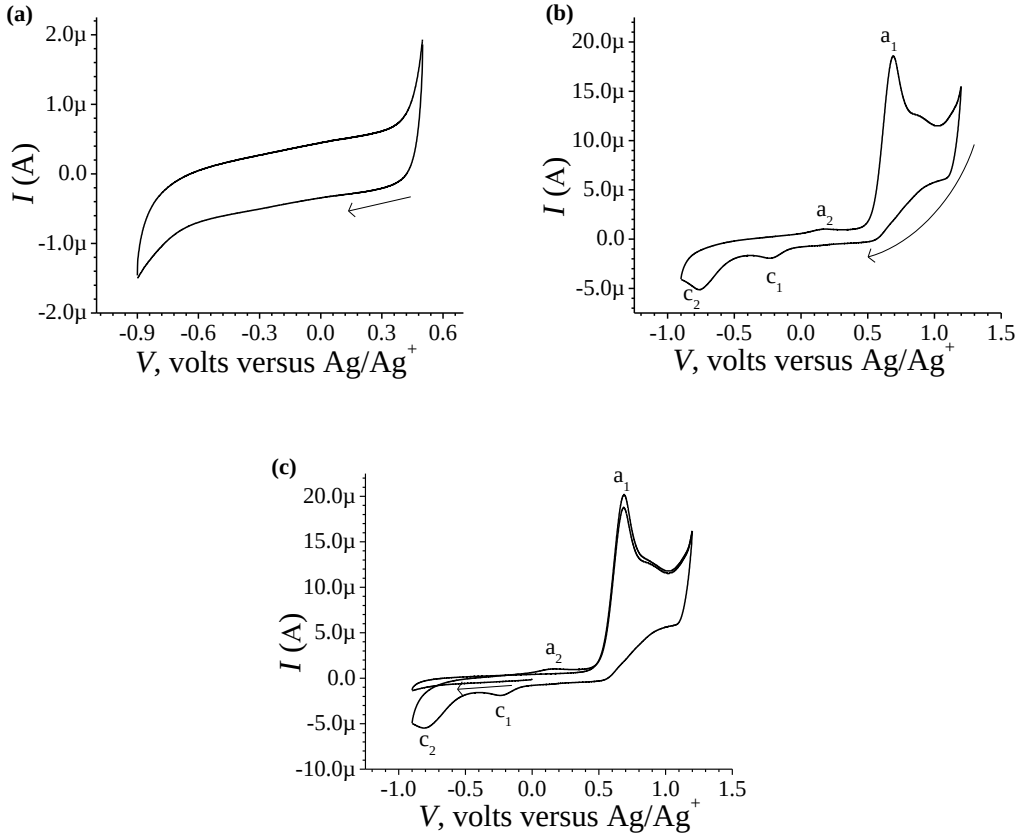

Figure 2.6 Cyclic voltammograms of **L_1** (1mM in DCM) using 0.1 M $TBAPF_6$ as the supporting electrolyte. **(A)** 0.5 V to -0.9 V **(B)** 1.2 V to -0.9 V and **(C)** 1.2 V to -0.9 V starting from 0.0 V

As can be seen from the Figure 2.6(a), no significant electrochemical activity is observed in the potential range of 0.5 V to -0.9 V. It is observed that [Fig. 2.6(c)] on scanning the potential from 0.0 V to -0.9 V, no cathodic process is observed, however an anodic peak appeared at 0.68 V, on reversal of scan direction from -0.9 V to 1.2 V. Finally in the second cycle of CV, from 1.2 V to -0.9 V and back to 1.2 V, two cathodic peaks, **c_1** at -0.2 V & **c_2** at -0.8 V and two anodic peaks, **a_1** at 0.68 V & **a_2** at 0.17 V were observed.

The cyclic voltammograms recorded at various scan rates (100 mV/sec to 500 mV/sec) revealed a small shift in peak potentials and increased peak heights with increase in scan rates. (Figure 2.7)

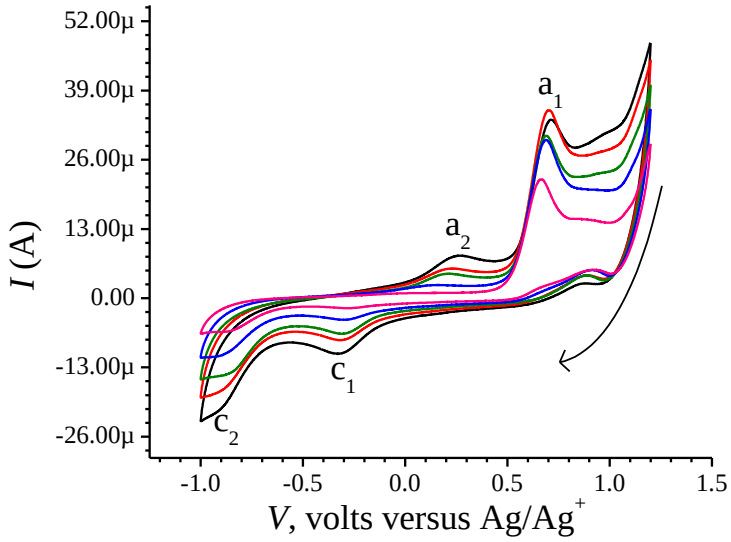

Figure 2.7 Cyclic voltammogram of the Betti base at increasing scan rate from 100 to 500 mV/sec

The plots of square root of scan rate vs. current [Fig. 2.8 (a-d)] gave straight lines for the reduction processes **c_1** and **c_2** indicating these processes to be diffusion controlled processes. However, the plots for oxidation i.e. **a_1** & **a_2** peak currents as a function of square root of scan rate deviated from linearity indicating existence of some other process along with electrochemical process.

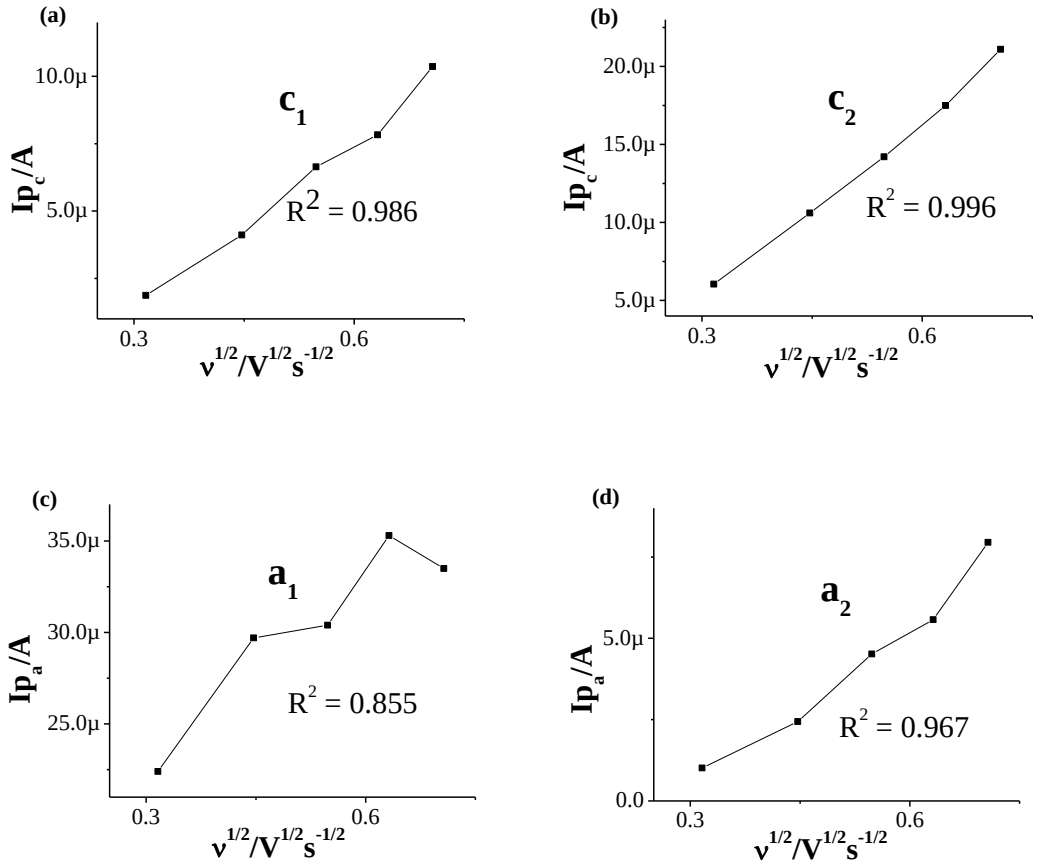

Figure 2.8 Plots of square root of scan rate vs. current **(a),(b)** cathodic current ; **(c),(d)** anodic current

To study effect of pH on the redox processes, CVs were recorded at three different pH conditions, which are depicted in Figure 2.9 which exhibits small changes in the peak potential values for the oxidation processes $\mathbf{a_1}$ & $\mathbf{a_2}$ and reduction process $\mathbf{c_2}$, however, the $\mathbf{c_1}$ reduction peak potential appears to be unaffected by the change in pH.

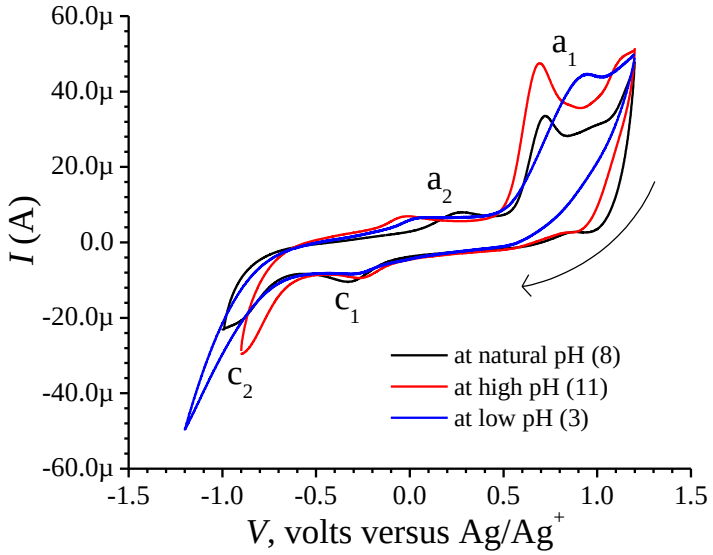

Figure 2.9 Cyclic voltammograms of a 1 mM solution of BB in DCM at 300 mV/sec containing 0.1 M $TBAPF_6$ as the supporting electrolyte.

The dependence of the overall redox process on the high positive values of the initial potential 1.2 V [Fig. 2.6(c)] indicates a need of overpotential to increase the charge transfer for oxidation. Thus the first step is formation of iminium ion, species **II,** by loss of two e^- and two protons at 0.69 V. As this involves loss of protons, the process is dependent on pH. This species exists in equilibrium with the protonated iminium ion **III** which is more stable and undergoes reduction at -0.31 V to form radical **IV** which is then further reduced to form benzylic carbanion **V**. The benzylic anion is quickly equilibrated with phenoxide.

The mechanism can be depicted as Scheme 2.16.

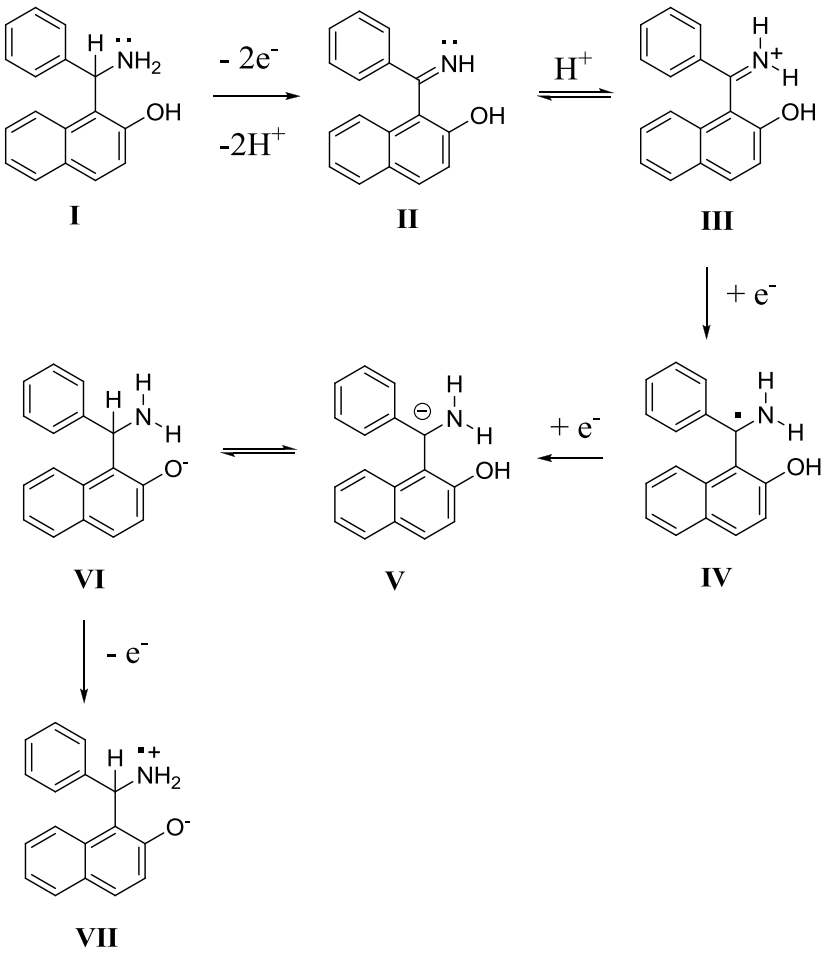

Scheme 2.16 Proposed mechanism for the redox reaction of Betti base.

2.4.3.2. Cyclic voltammetric study of PBB (L_4) and DBB (L_7)

The cyclic voltammograms of PBB (**L_4**) (1.0 mM in DCM) recorded at different scan rates (100-500 mV/sec) in the potential window of 1.2 V to -1.0 V are shown in Figure 2.10. The increase in peak current and shift in the peak potential were observed with increasing the scan rate from 100-500 mV/sec. The plots of square root of scan rate vs. cathodic and anodic current are given Figure 2.11.

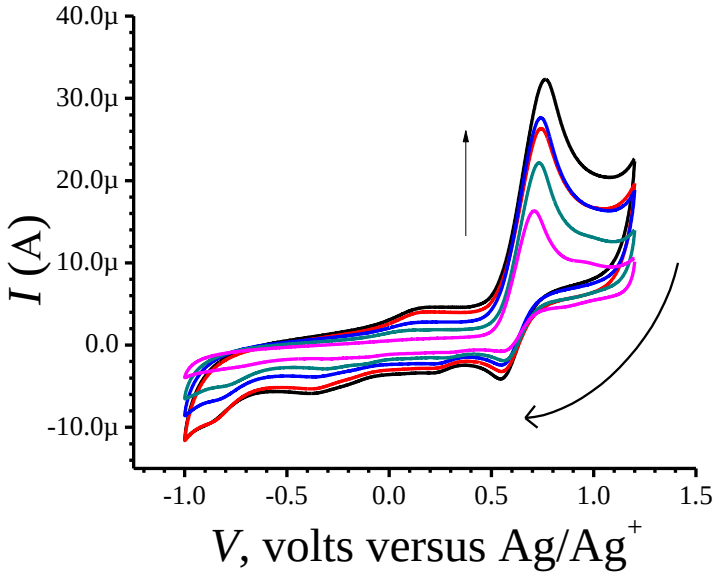

Figure 2.10 CVs of **L4**

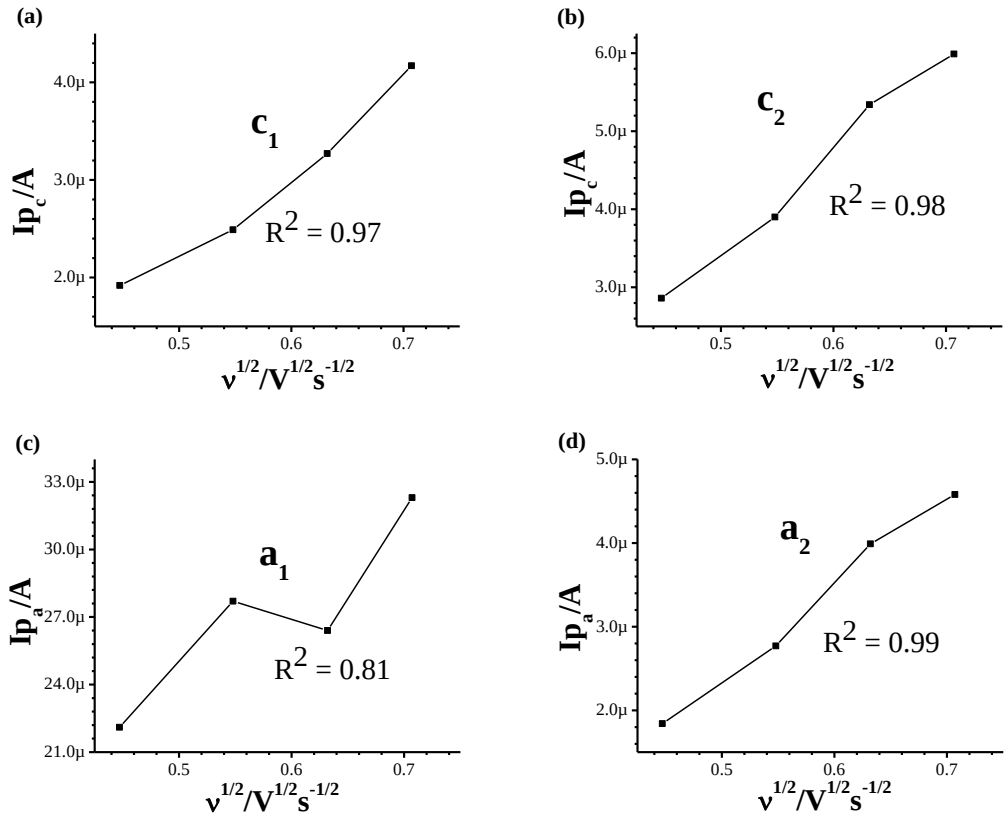

Figure 2.11 Plots of current vs. scan rate

The lines with R^2 values ~0.99 for the redox processes **c_1**, **c_2** and **a_2** indicate diffusion controlled redox process However, the oxidation process **a_1** is not diffusion controlled, indicating the existence of some other process along with electrochemical process.

To check the effect of pH over redox process, the CV was recorded at high pH (11.0) (Fig. 2.12). As can be seen from the Figure 2.12 no change in reduction potentials were observed for the reduction processes **c_1** and **c_2** whereas shift in the oxidation potentials of the oxidation processes **a_1** and **a_2** are observed.

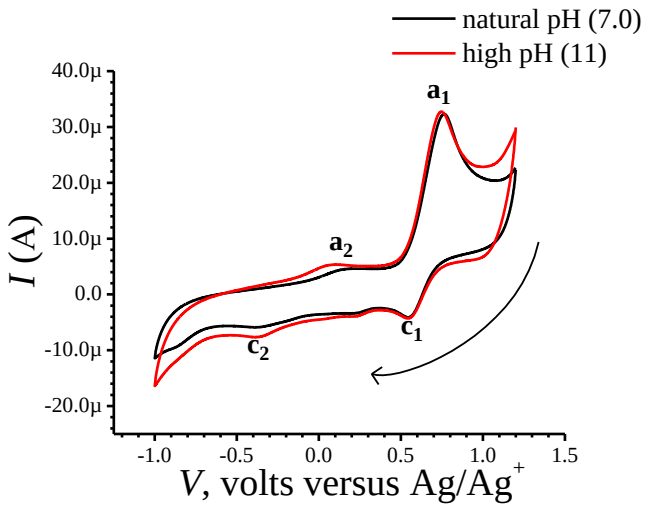

Figure 2.12 CVs of **L_4** at different pH

The cyclic voltammogram of DBB (**L_7**) (1.0 mM in DCM, 600 mV/sec) in the potential window of 1.2 V to -1.0 V is shown in Figure 2.13.

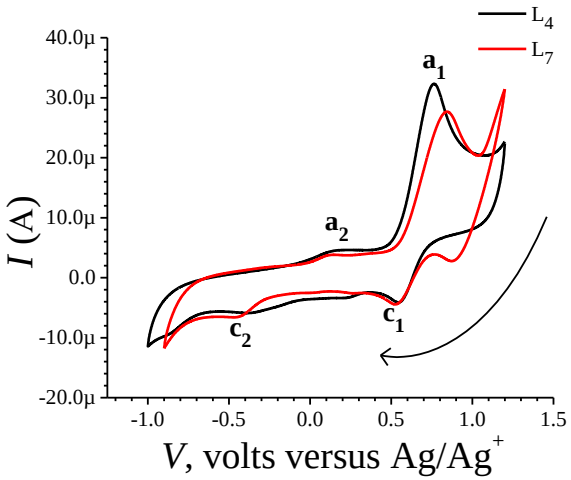

Figure 2.13 CV of **L_4** and **L_7**

As can be seen from the Figure 2.13, the CV of **L7** was observed to be similar to that of **L4**.

To check the effect of pH over redox process, the CV was recorded at high pH (11.0) (Fig. 2.14). As can be seen from the Figure 2.14 no change in reduction potentials were observed for the reduction processes **c1** and **c2** whereas shift in the oxidation potential of the oxidation processes **a1** and **a2** was observed.

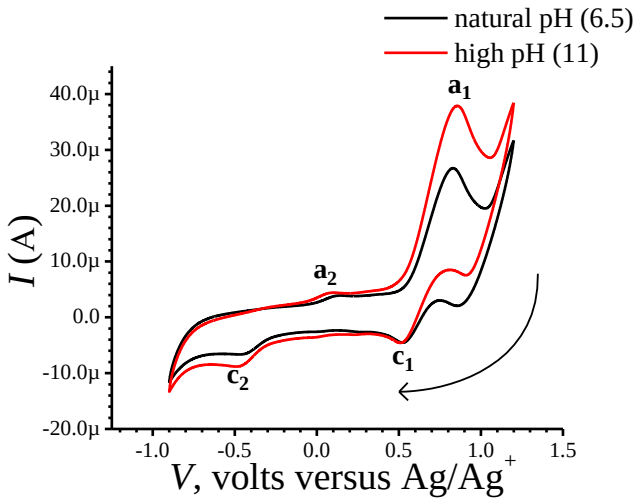

Figure 2.14 CVs of **L7** at different pH

From the cyclic voltammograms obtained for **L4** and **L7** and the redox potential values as given in Table 2.1 it can be concluded that redox process involved in **L4** and **L7** is somewhat different than that observed in **L1**. These observations forced us to compare the results obtained with reported results for similar systems.

As mentioned previously in the introduction of this chapter, the electrochemical behavior of amino phenols has been extensively studied by Matsumura et al. and Thomas et al. [23] (Fig. 2.15)

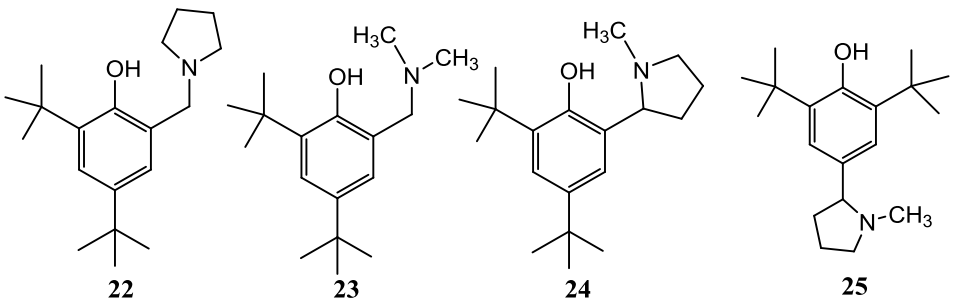

Figure 2.15 Structures of the α-alkyl amino phenol derivatives

The similarities in the structures of the amino phenols **22** & **23** with that to the ligand **L4** and **L7** used in the present study is noteworthy, though the substituent on the phenolic benzene rings are different as given in Table 2.2 below.

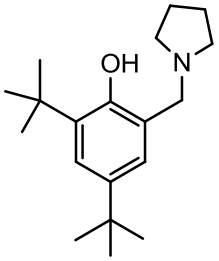 **22**	Redox potentials of **22** Epa = 0.85 V Epc = 0.67 V	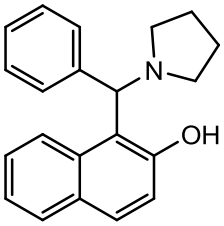 **L4**	Redox potentials of **L4** Epa = 0.74 V Epc = 0.55 V
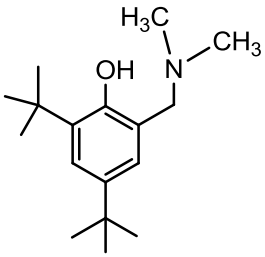 **23**	Redox potentials of **23** Epa = 0.82 V Epc = 0.69 V	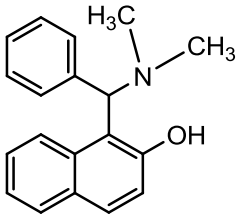 **L7**	Redox potentials of **L7** Epa = 0.82 V Epc = 0.52 V

Table 2.2 Redox potentials of amino phenols and amino naphthols

On the basis of DFT, CV, UV-Visible and EPR studies the redox mechanism for the amino phenols **22** and **23** have been proposed by Matsumura et al. (Scheme 2.17) which has been further confirmed by other research groups. [24-33]

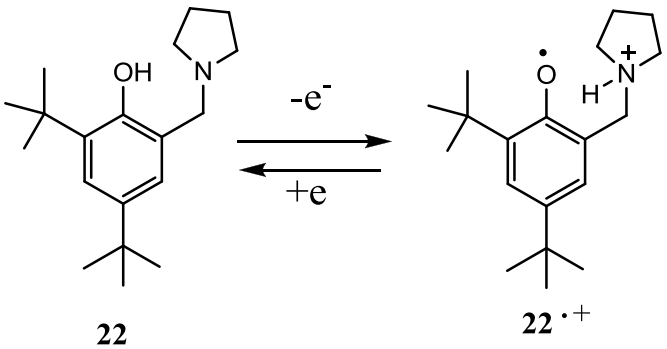

22 **22**$^{\bullet+}$

Scheme 2.17 Proposed redox process of **22/22**$^{\bullet+}$ through iminium proton migration

As discussed in detail by Saveant et al. [25,34] for the electrochemical reactions of the amino phenols, there are two possible pathways namely 1) electron followed by proton transfer (EPT) and 2) proton followed by electron transfer (PET) However, scientists have now proved through detailed analysis of CV that the process follows concerted proton electron transfer pathway (CPET) also known as proton coupled electron transfer (PCET) (Scheme 2.18).

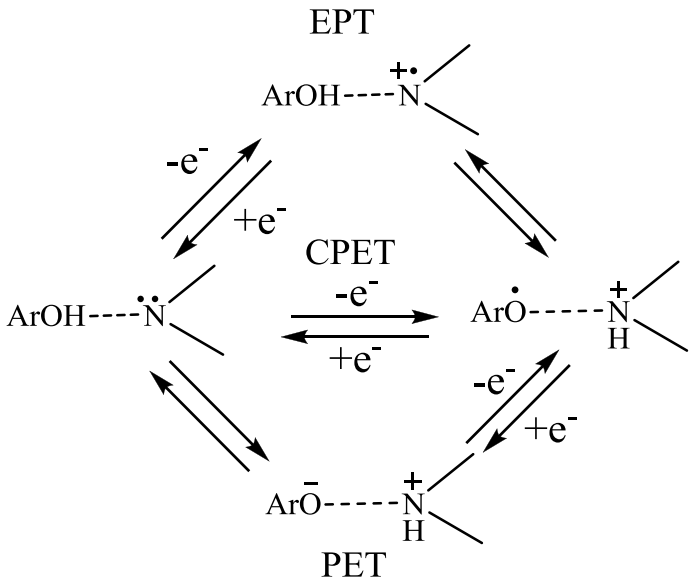

Scheme 2.18 Pathways for the redox reaction of amino phenols

The CV of ligand **L4** & **L7** with tertiary amine indicated somewhat similar behavior as that of **22 & 23**. The initial potential required for the oxidation step is high and this nature is matching with the values reported for the oxidation of **22** and **23** by Matsumura et al.[23]

According to the Scheme 2.17 the redox mechanisms for the ligands **L4** and **L7** have been proposed likewise (Scheme 2.19 & 2.20).

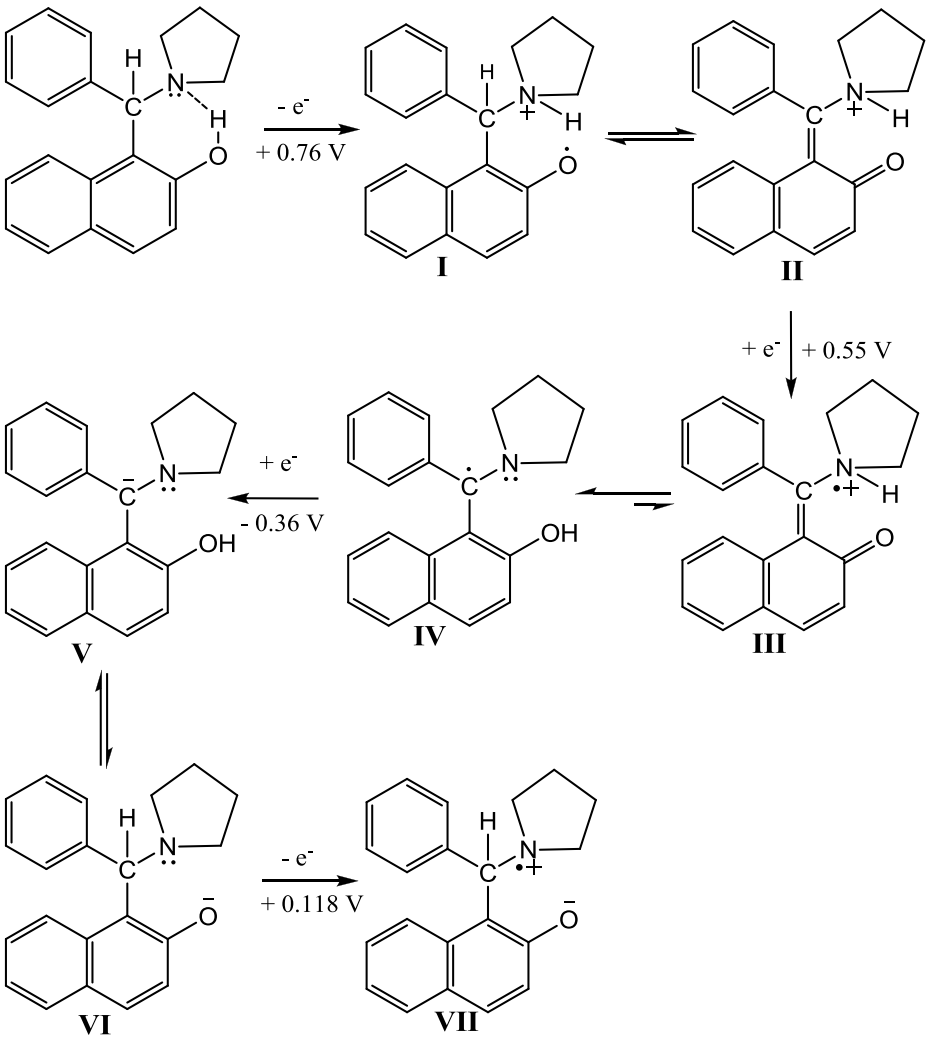

Scheme 2.19 Proposed redox mechanism for ligand **L4**

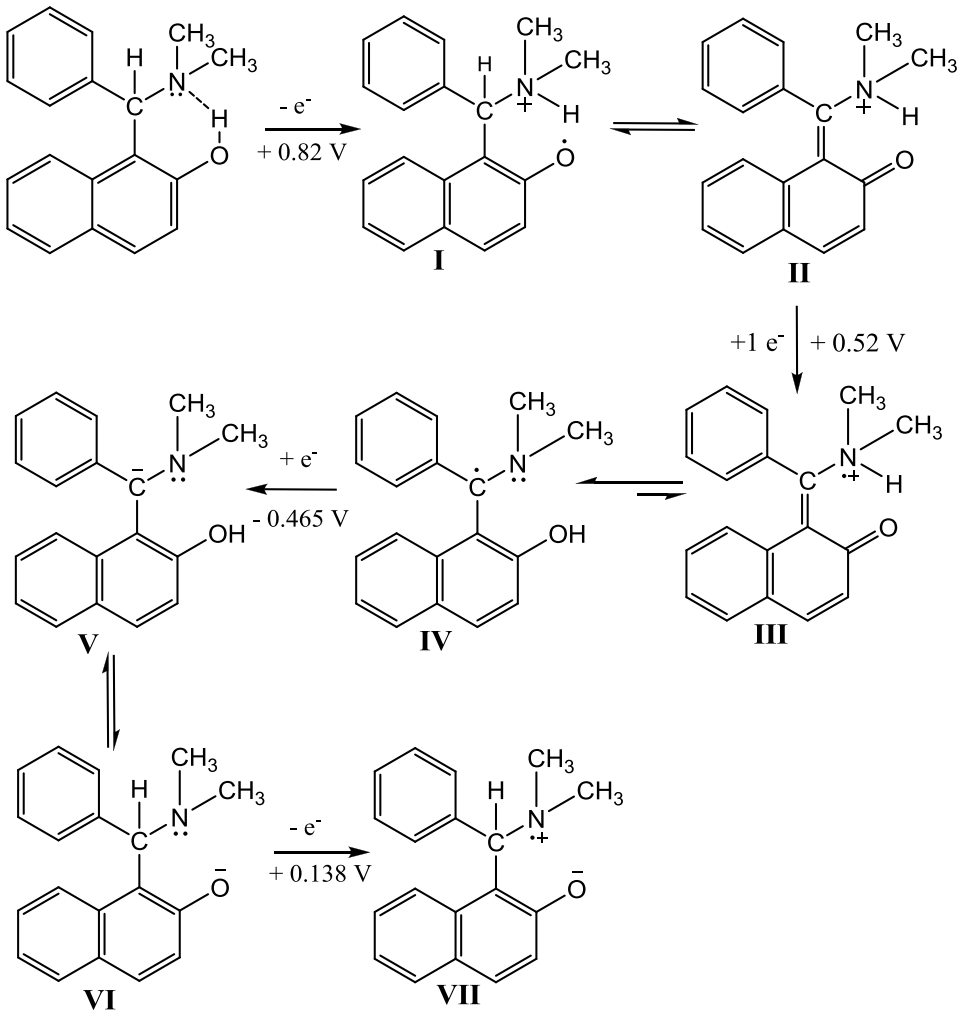

Scheme 2.20 Proposed redox mechanism for ligand **L_7**

The first step is the formation of **$L_4^{\bullet+}$ (I)** by loss of an $-e^-$ and migration of proton through CPET pathway at 0.76 V (**a_1** Fig. 2.12). The step involved in migration of proton would certainly be dependent on pH condition which was observed by shift in the oxidation potential in CV taken at high pH (Fig. 2.12). The species **I** transforms into species **II** through activation of sp^3–C–H bond α to nitrogen. [41,42] The species **II** reduced at 0.55 V to form species **III** (**c_1** Fig. 2.12). The species **III** quickly regain its aromaticity to form stable benzylic radical **IV**. The radical **IV** is further reduced to form a benzylic carbanion **V** at –0.36 V (**c_2** Fig. 2.12) which is expected to quickly equilibrate to phenoxide **VI**. The species **VI** is oxidized at 0.12 V to form species **VII**.

2.4.4. Elimination Voltammetry

Identification of the nature of currents involved in the electron transfer process i.e. diffusion, kinetic or adsorptive would augment the understanding of the process. Many mathematical models have been proposed to extract useful information from the CV data [43] and elimination voltammetry is one such model. Elimination voltammetry with linear scan (EVLS), an electrochemical method comprising the elimination of some particular currents from the measurements of linear scan voltammetry was first proposed by Dracka and simultaneously verified by Trnková in 1996. [44,45] A large volume of work has been published by Trnková et al. [45-52] Most of these papers point to EVLS as an excellent tool to understand electrochemical processes. It is successfully employed in the analysis of nucleic acids and short homo – or hetero – deoxyoligonucleotides (ODNs) containing adenine and cytosine. [52-54]

Libuše Trnková

Cyclic voltammogram consist of combination of various currents like diffusion , charging and kinetic and so forth

2.4.4.1. Diffusion current

A faradaic current whose magnitude is controlled by the rate at which an electroactive species diffuses toward an electrode-solution interface (and, sometimes, by the rate at which a product diffuses away from that interface). ***Diffusion current varies with square root of the scan rate.***

2.4.4.2. Kinetic current

A faradaic current that corresponds to the electroreduction or electrooxidation of an electroactive substance formed by a prior chemical reaction from another substance that is not electroactive. Kinetic current is partially or entirely controlled by the rate of the chemical reaction. This reaction may be heterogeneous, occurring at an electrode-solution interface (surface reaction), or it may be homogeneous, occurring at some

distance from the interface (bulk reaction).

2.4.4.3. Charging / Adsorption current

The non-faradic current associated with the charging of the electrical double layer at an electrode-solution interface. ***Charging current is directly proportional to the scan rate.***

2.4.5. Theory of Elimination voltammetry

The EVLS can be considered as a transformation of current – potential curves capable of eliminating some selected current components, while conserving others by means of elimination functions. [44,55] The elimination function is based on rate dependence of various currents *i.e.* diffusion current, kinetic current, charging current etc. Let I be the total reference current measured at reference scan rate ν_{ref} and $I_{1/2}$ & I_2, the total currents measured at scan rates equal to one half and twice of the reference current scan rate ν_{ref}, respectively. The total currents recorded at the scan rates $(1/2)\ \nu_{ref}$, ν_{ref}, and $2\nu_{ref}$ can be given as

$$I_{1/2} = (I_d)_{1/2} + (I_c)_{1/2} + (I_k)_{1/2}$$

$$I = (I_d) + (I_c) + (I_k) \qquad (1)$$

$$I_2 = (I_d)_2 + (I_c)_2 + (I_k)_2$$

Elimination is produced by the construction of a function of the total current $f(I)$ in the form of a linear combination of total currents, measured at different scan rates , and can be expressed as:

$$f(I)=a_1 I_{1/2}+a_2 I+a_3 I_2. \qquad (2)$$

With respect to nature of the simple currents shown, only the ratio of scan rate ν to the reference scan rate ν_{ref} is important. The total currents used in linear combination are then marked with an index expressing ν/ν_{ref} ratios, so I_2, is the total current for $\nu/\nu_{ref} = 2$, etc and can be expressed as:

$$a_1 I_{1/2} = a_1 (1/2)^{1/2}(I_d) + a_1 (1/2)(I_c) + a_1 (I_k)$$

$$a_2 I = a_2 (I_d) + a_2 (I_c) + a_2 (I_k) \quad (3)$$

$$a_3 I_2 = a_3 (2)^{1/2} (I_d) + a_3 (2)(I_c) + a_3 (I_k)$$

For the conservation of diffusion current with simultaneous elimination of kinetic and charging currents the following requirements should be fulfilled.

$$a_1(1/2)^{1/2}(I_d) + a_2(I_d) + a_3(2)^{1/2}(I_d) = I_d,$$

$$a_1(1/2)(I_c) + a_2(I_c) + a_3(2)(I_c) = 0, \quad (4)$$

$$a_1(I_k) + a_2(I_k) + a_3(I_k) = 0,$$

The coefficients a_1, a_2, and a_3 can be obtained by solving above three equations simultaneously using Matlab program [46,56] and their values are calculated as

$$a_1 = -11.657;\ a_2 = 17.485;\ a_3 = -5.8284. \quad (5)$$

Hence the elimination function for conservation of diffusion current with simultaneous elimination of kinetic and charging current can be given as E4 [44], simultaneous elimination of I_k and I_c, with conservation of I_d:

$$E4 = -11.657\ I_{1/2} + 17.485\ I - 5.8284\ I_2 \quad (6)$$

Same way for the elimination of charging current with the conservation of diffusion & kinetic current, and for the elimination of diffusion current with the conservation of kinetic & charging current the general equation which can be used is

$$f(I) = a_1 I_{1/2} + a_2 I \quad (7)$$

Hence for the conservation of diffusion & kinetic current following requirements should be fulfilled

$$a_1(1/2)^{1/2}(I_d) + a_2(I_d) = I_d,$$
$$a_1(1/2)(I_c) + a_2(I_c) = 0, \quad (8)$$
$$a_1(I_k) + a_2(I_k) = I_k,$$

Similarly, for the conservation of kinetic & charging current the equation (8) can be written as

$$a_1(1/2)^{1/2}(I_d) + a_2(I_d) = 0 ,$$
$$a_1(1/2)(I_c) + a_2(I_c) = I_c, \quad (9)$$
$$a_1(I_k) + a_2(I_k) = I_k,$$

The coefficients a_1 and a_2 can be obtained by using Matlab program [46,56] and their values for the equations (8) & (9) are shown in the equation (10) respectively.

$$a_1 = 4.8284;\ a_2 = -2.4142 \quad (10)$$
$$a_1 = 3.4142;\ a_2 = -2.4142$$

Hence the elimination function for conservation of diffusion & kinetic currents with elimination of charging current can be given as E2 [44], elimination of I_c with conservation of I_d & I_k

$$E2 = 4.8284\ I_{1/2} - 2.4142\ I \quad (11)$$

The elimination function for conservation of kinetic & charging currents with elimination of diffusion current can be gives as E3 [44], elimination of I_d with conservation of I_k & I_c

$$E3 = 3.4142\ I_{1/2} - 2.4142\ I \quad (12)$$

As a result of elimination, the reversible current of a substance transported to an electrode surface by diffusion only, is improved giving sharp peaks for reduction or oxidation signals. For the irreversible current of a fully adsorbed substance, this function provides the characteristic signal of a peak-to-counterpeak form, improving strongly the resolution and sensitivity. [44, 51, 52, 55, 57, 58] Thus for the application of elimination voltammetry, all that is needed is voltammetric data at three scan rates. Once this data is fed in to an appropriate elimination equation in MS excel program, it generates information that is useful for understanding of the electrochemical processes.

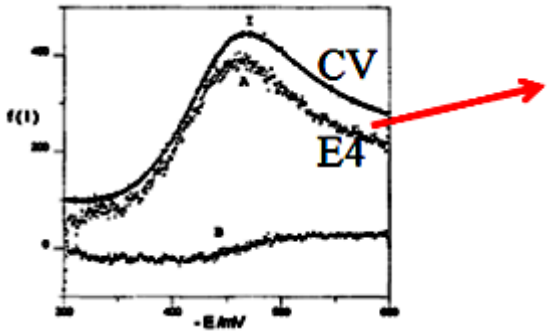

The E4 current equal to CV current indicates reversible diffusion controlled process.

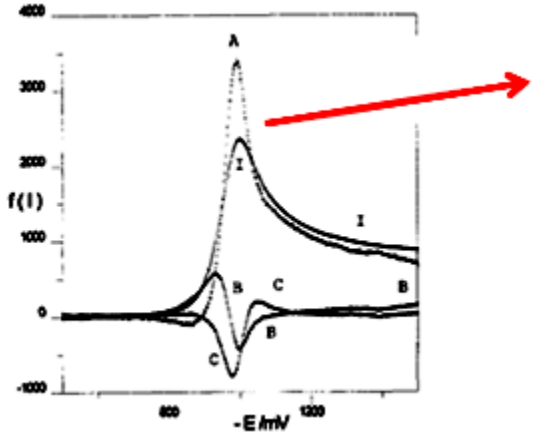

The E4 current is higher than CV current indicates quasi irreversible diffusion controlled process.

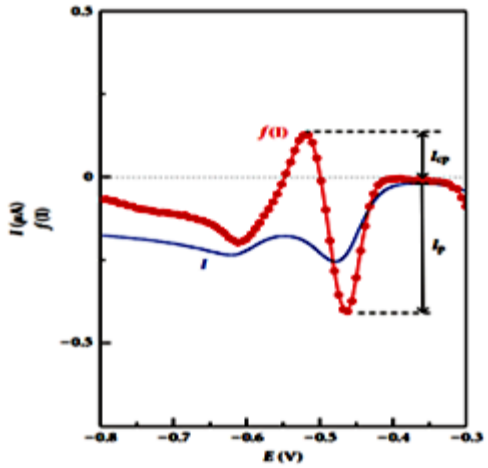

The observation of peak – counter peak current on application of E4 function indicates electron transfer process proceeding in the adsorbed state of electroactive species.

The simplicity and sensitivity of the elimination tool prompted us to explore its application to study electrochemical behavior of Bettibase and its derivatives.

2.4.6. Data Treatment for Elimination voltammetry

The voltammetric data were collected using CH600C Potentiostat instrument and exported to MS Excel for processing of elimination functions. The elimination functions E2, E3 & E4, have been used for the evaluation of measurement. For the sake of simplicity, the overlay curves of elimination functions (E2, E3, E4) and CV for the forward and reverse scans are displayed separately.

2.4.6.1. Elimination Voltammetric analysis of Betti base (L_1)

The elimination functions E4, E2 and E3 for oxidation and reduction at different pH are given in the Figures below [Figure 2.16 –2.19].

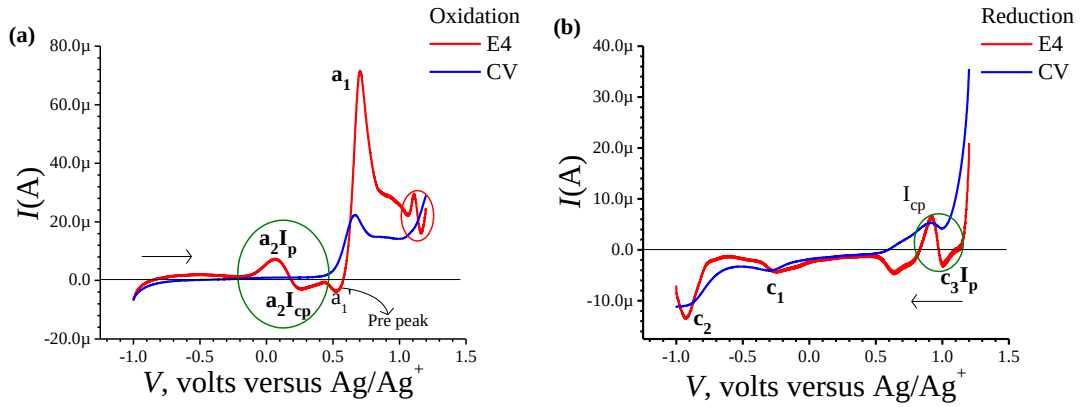

Figure 2.16 E4 Plots for **(a)** Oxidation process **(b)** Reduction process of Betti base

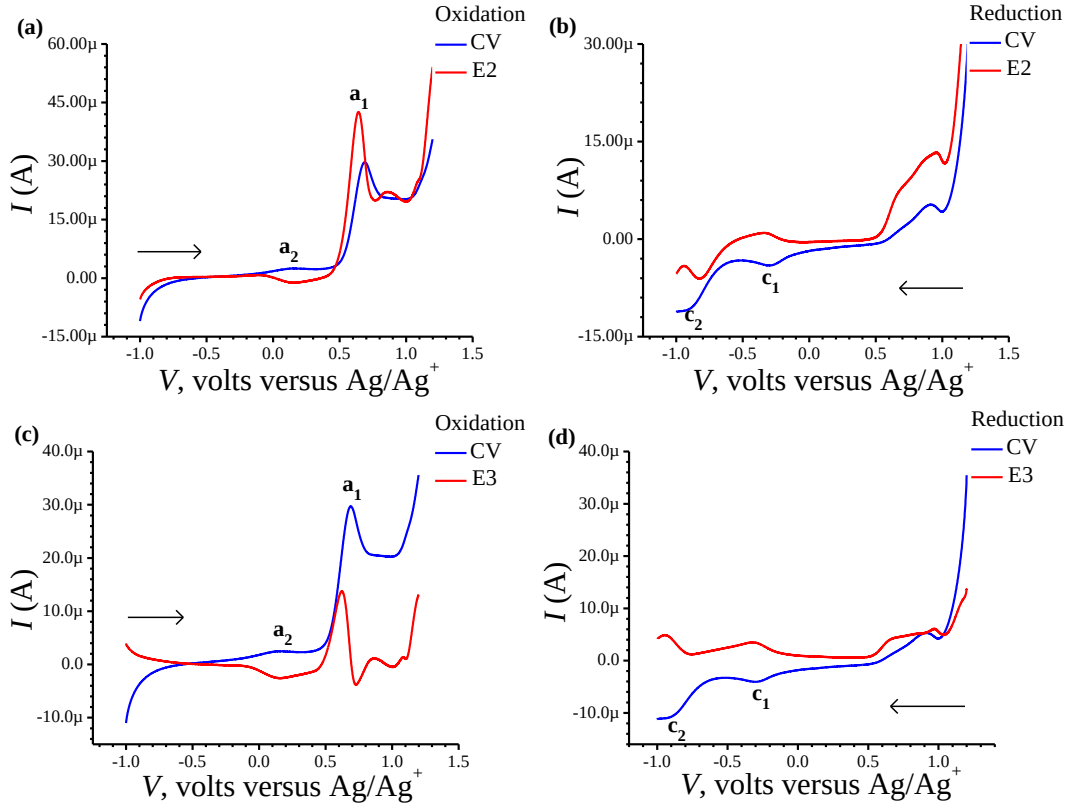

Figure 2.17 E2 Plots for **(a)** oxidation of Betti base **(b)** reduction of Betti base;
E3 Plots for **(c)** oxidation of Betti base **(d)** reduction of Betti base

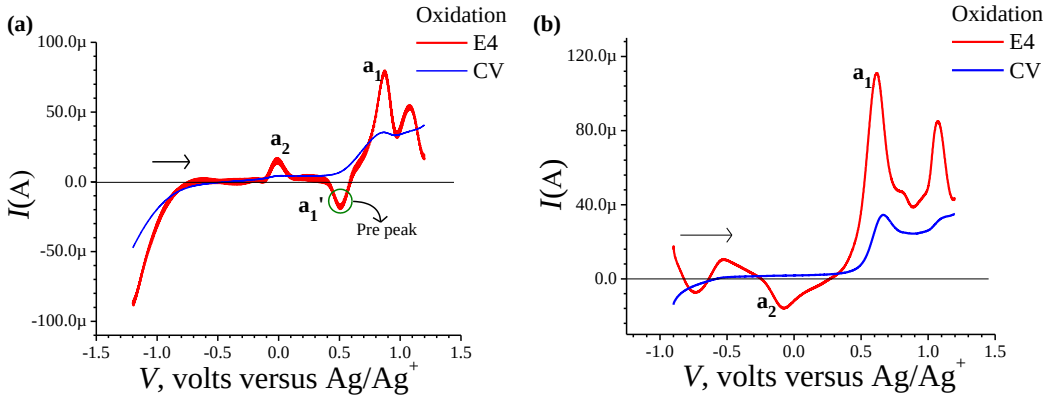

Figure 2.18 E4 Plots for **(a)** Oxidation process at low pH of Betti base **(b)** Oxidation process at high pH of Betti base

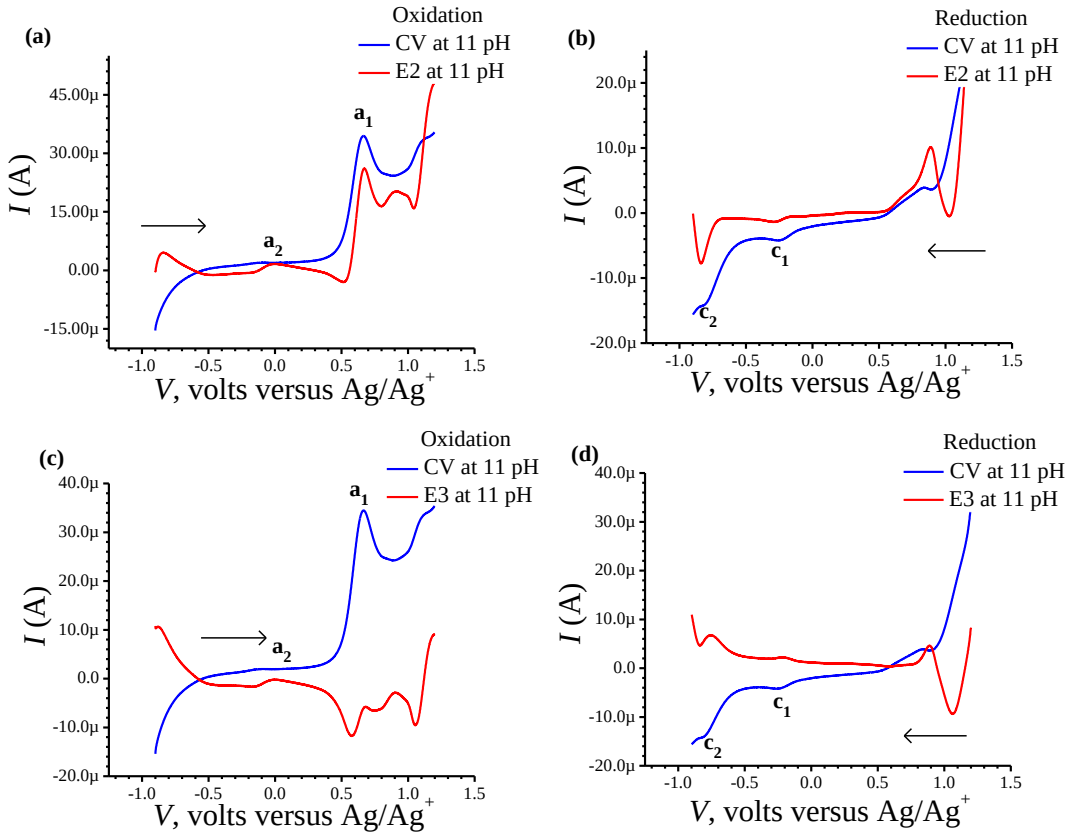

Figure 2.19 E2 Plots for Betti base at high pH **(a)** oxidation **(b)** reduction;
E3 Plots for Betti base at high pH **(c)** oxidation **(d)** reduction

The redox mechanism for Betti base, proposed previously (Scheme 2.16) can be correlated with the elimination voltammetry results.

The first step i.e. formation of a species **II** (**a_1**) might be controlled by either a mass transport diffusion processes or a preceding chemical reaction associated with the charge transfer reaction giving kinetic current or may be a combination of both. The appearance of the prepeak **a_1'** [Fig. 2.16(a)] in the elimination curve E4 may be due to proton transfer followed by electron transfer. This is further confirmed by the pH dependence of peak **a_1** in the CV [Fig. 2.9] and appearance of prepeak **a_1'** in the EVLS curves [Fig. 2.16(a),]. At high pH, the formation of naphthoxide species is favorable so the oxidation potential of peak **a_1** should shift to lower value which is observed. A complete disappearance of the prepeak **a_1'** and increased height of the peak **a_1** at alkaline pH in the EVLS [Fig. 2.18(b)] hint towards a possibility of simultaneous transfer of proton and electron. The elimination functions E2 which represents elimination of charging and conservation of kinetic and diffusion appeared as distorted peak at **a_1** and the E3 which represents elimination of diffusion and conservation of kinetic and charging resulted in a peak opposite to the one observed at **a_1** in CV supported the proposed electrochemical process at **a_1** i.e. transfer of electron and proton. These functions also exhibit pH dependence as anticipated obviously [Fig. 2.9]

The elimination function applied to the data for the reversed scans of CV resulted in two peaks, **c_1** with no change in peak height and **c_2** with a small increase in peak height [Fig. 2.16(b)]. Apart from these two peaks, application of the E4 function resulted in a small peak – counter peak at **c_3** [Fig. 2.16(b)]. This is attributed to strong adsorption of the species on the electrode surface. The reduction processes at **c_1** and **c_2** are predicted to be irreversible diffusion controlled processes from the mechanism and it is supported by the appearance of peaks at **c_1** and **c_2** in the E4 plots [Fig 2.16 (b)].

The elimination functions E2 and E3 also corroborate the suggested mechanism as sharp peak with lower height appeared in E2 and peaks in opposite direction to that of CV appeared in E3.

Thus the elimination volatmmetric analysis of the data helped in better understanding of the electrochemical process of Betti base.

2.4.6.2. Elimination Voltammetric analysis of PBB (L_4)

The redox process of ligand PBB (**L_4**) has been studied through elimination voltammetry. The overlay curves of elimination functions (E2, E3, E4) and CV for the forward and reverse scans are displayed separately [Figure 2.20(a-b) and Figure 2.21 (a-d)]

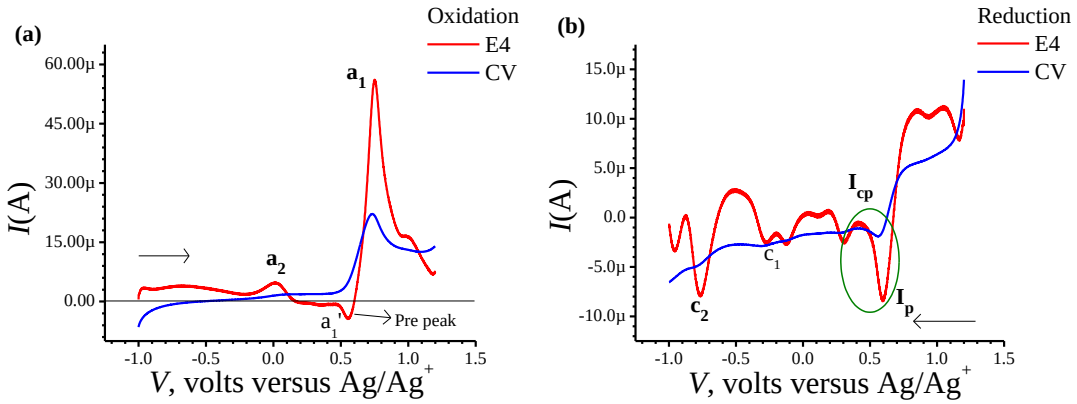

Figure 2.20 E4 Plots for for PBB **(a)** Oxidation process **(b)** Reduction process

The appearance of prepeak-peak (**a_1'**) in the E4 function curve for oxidation at **a_1** indicates kinetic and diffusion currents as expected for the loss of electron followed by intraligand proton transfer. To confirm this, E2 and E3 plots were plotted as shown in the Figure 2.21 (a-d).

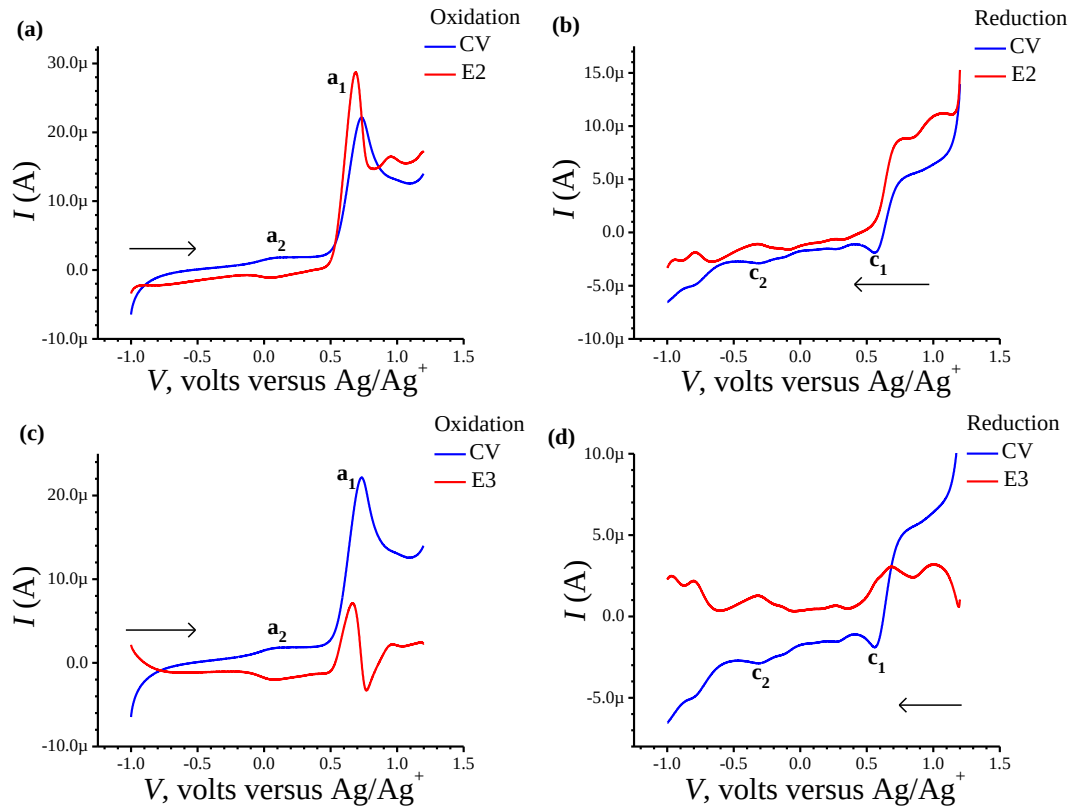

Figure 2.21 Plots for elimination functions **E2** (a) oxidation of PBB (b) reduction of PBB ; plots for the elimination function **E3** (c) oxidation of PBB (d) reduction of PBB

The increased peak height of $\mathbf{a_1}$ indicates diffusion with the effect of kinetics whereas decreased or the distorted peak in the E3 function at $\mathbf{a_1}$ indicates that the process corresponds to kinetics as the diffusion current (I_d) is eliminated. The E4, E2 and E3 functions at high pH overlaid with CV plots are shown in Figure 2.22. (a-b) and Figure 2.23 (a-d)

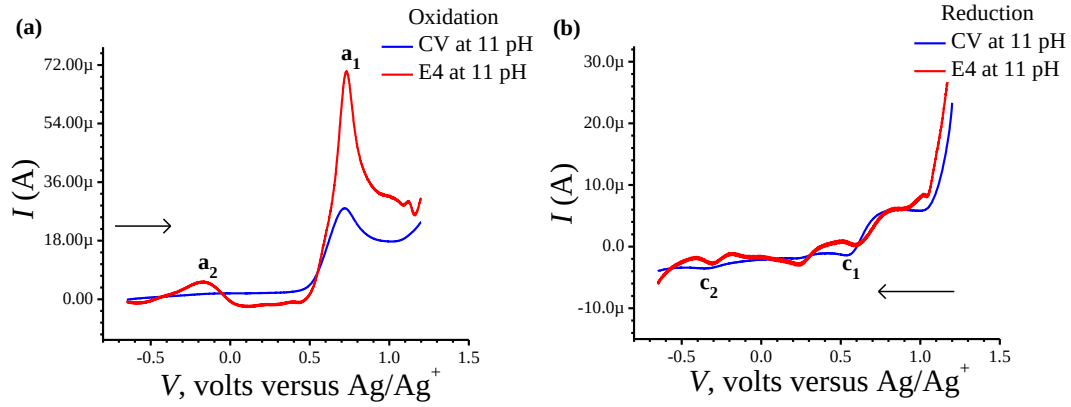

Figure 2.22 Plots for diffusion current I_d for PBB at high pH **(a)** Oxidation process **(b)** Reduction process

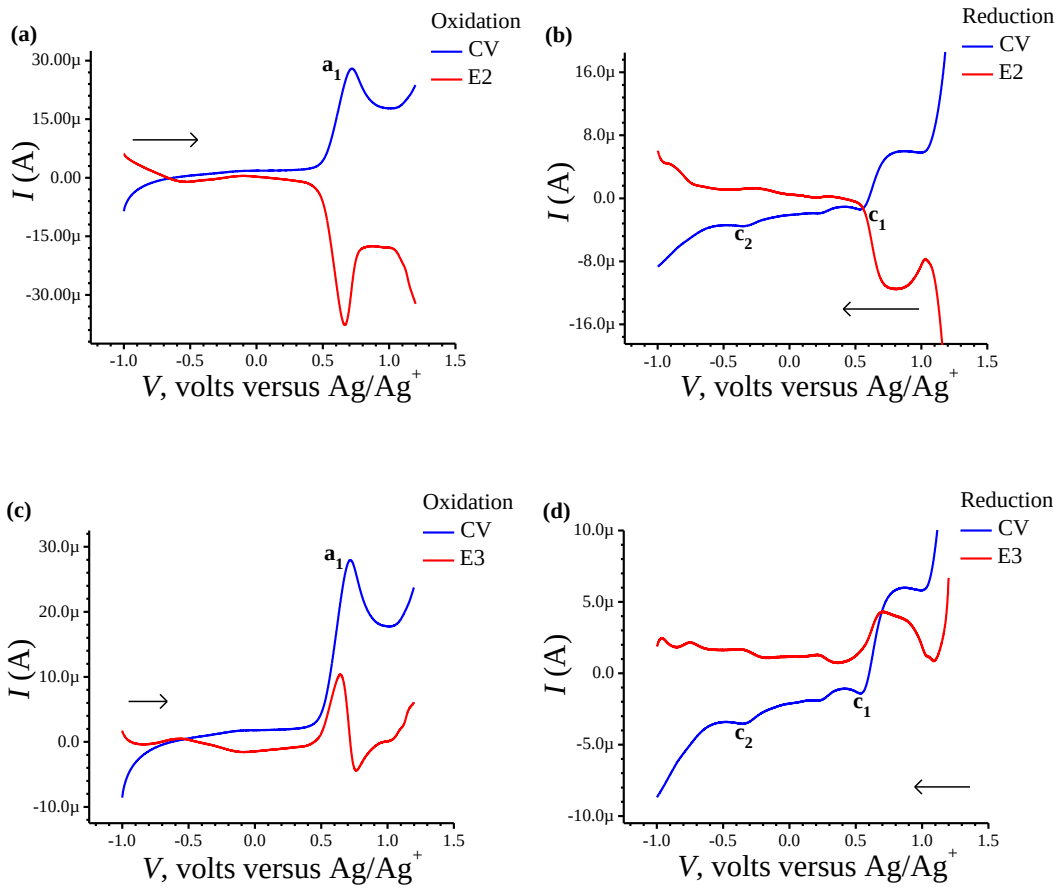

Figure 2.23 Plots for elimination functions **E2** at high pH (a) oxidation of PBB (b) reduction of PBB ; plots for the elimination function **E3** at high pH (c) oxidation of PBB (d) reduction of PBB

The nature of E4, E2 and E3 function once again support the proposed mechanism which involves formation of ammonium cation.

The elimination function applied to the data for the reversed scans of CV resulted in multiple peaks. Both the reduction peaks $\mathbf{c_1}$ and $\mathbf{c_2}$ are split into two peaks with no change in peak height for $\mathbf{c_1}$ and with a small increase in peak height for $\mathbf{c_2}$ [Fig. 2.20(b)]. Apart from these two peaks, application of the E4 function resulted in a peak – counter peak I_p–I_{cp} [Fig. 2.20(b)] indicating diffusion process of an adsorbed species.

These results indicated irreversible diffusion process as predicted for the reduction of the oxidized PBB.

2.4.6.3. Elimination voltammetric analysis of DBB (L_7)

The overlaid E4 and CV curve of ligand DBB are shown in Figure 2.24 (a) & (b). The elimination procedure resulted in a peak **(a_2)** and a prepeak-peak **(a_1' & a_1)** [Fig. 2.24(a)]. The decrease in current for the pre–peak **a_1'** indicated diffusion with kinetic process at the electrode surface. This is as predicted for the oxidation of DBB, which involves loss of electron followed by intra ligand proton transfer to give ammonium cation.

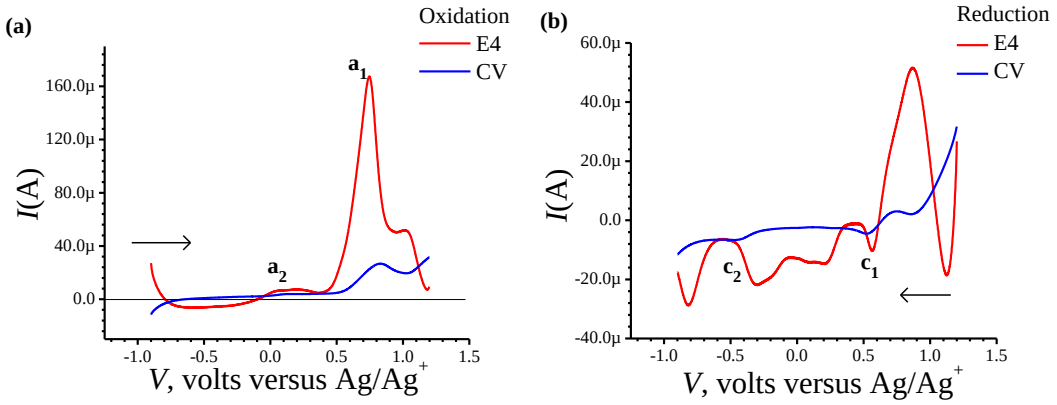

Figure 2.24 E4 Plots for DBB **(a)** Oxidation process **(b)** Reduction process

The elimination function applied to the data for the reversed scans of CV resulted in multiple peaks, with negligible increase in the peak current for **c_1** and substantial increase in peak current for **c_2** [Fig. 2.24(b)]. These results are once again as expected for reduction of the oxidized DBB.

Thus the elimination voltametric analysis supported the predicted mechanism for the redox process of DBB (L_4), which is similar to that of PBB (L_7).

2.4.6.4. Elimination voltammetric analysis of ABB (L_8)

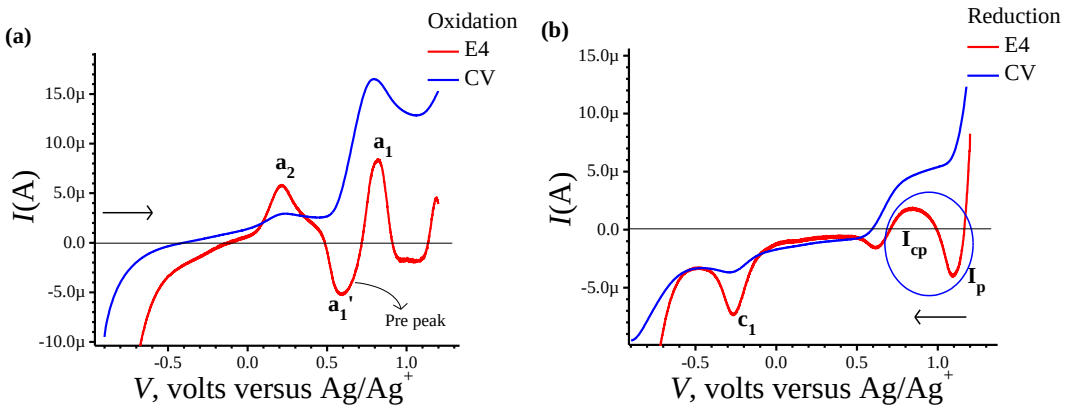

Figure 2.25 E4 Plots for ABB **(a)** Oxidation process **(b)** Reduction process

The overlaid E4 and CV curve of ligand ABB are shown in Figure 2.25 (a) & (b). The elimination procedure resulted in a peak **(a_2)** and a prepeak- peak **(a_1' & a_1)** [Fig. 2.25(a)]. The elimination function applied to the data for the reversed scans of CV resulted in a reduction peak **c_1** with substantial increase in the peak current [Fig. 2.25(b)]. Apart from this the application of the E4 function resulted in a peak – counter peak I_p–I_{cp} [Fig. 2.25(b)]. These observations are similar to that for BB (L_1) as expected and a similar conclusion can be drawn.

2.5. Conclusion

The combination of CV and elimination voltammetry has emerged as an amazing tool to identify the redox processes of electroactive compounds. It can be concluded from the CV and EVLS data that the Betti base and its derivatives are electroactive and undergo irreversible redox process.

2.6. Supporting information

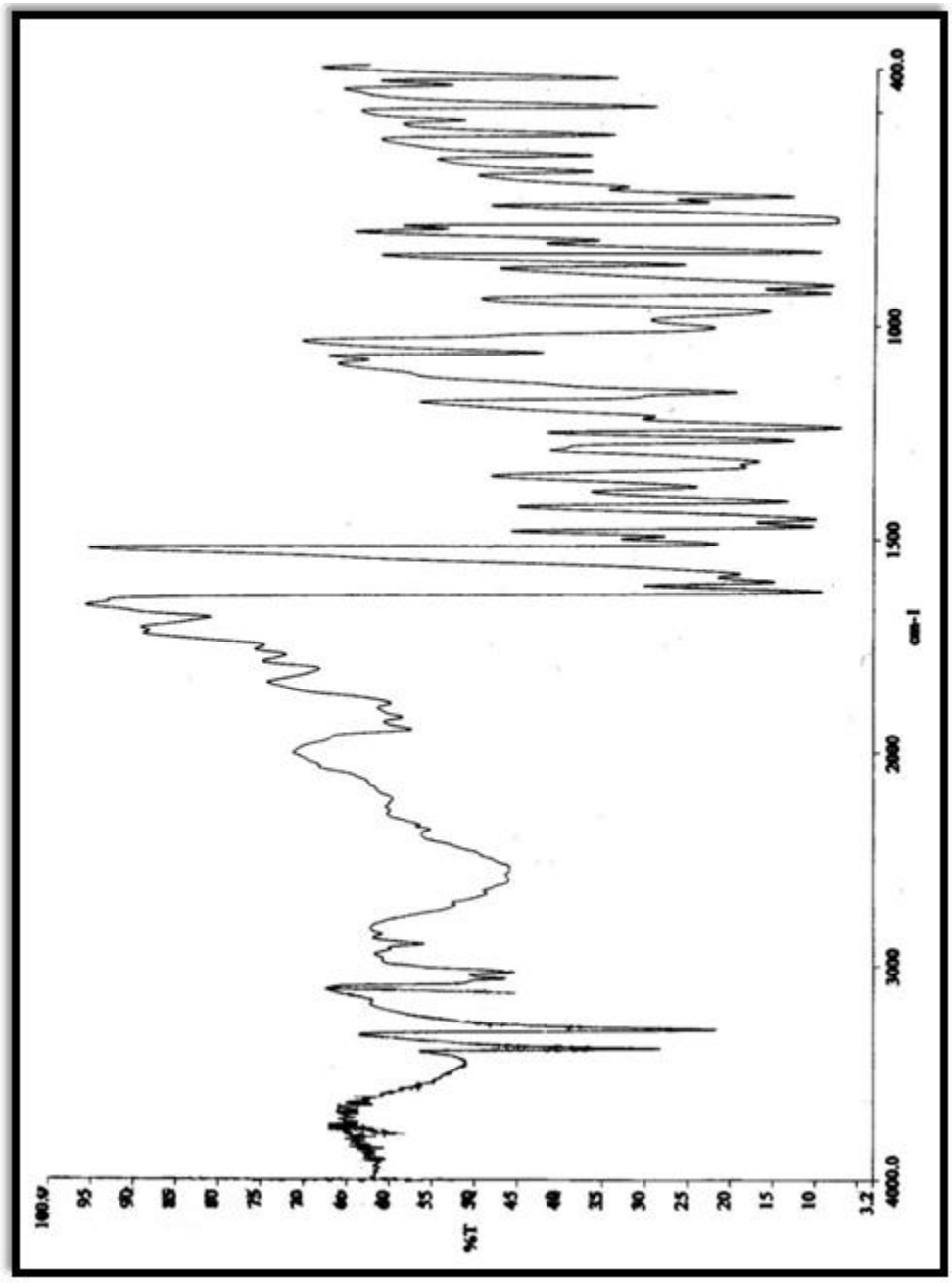

2.1SI FT-IR spectrum of BB

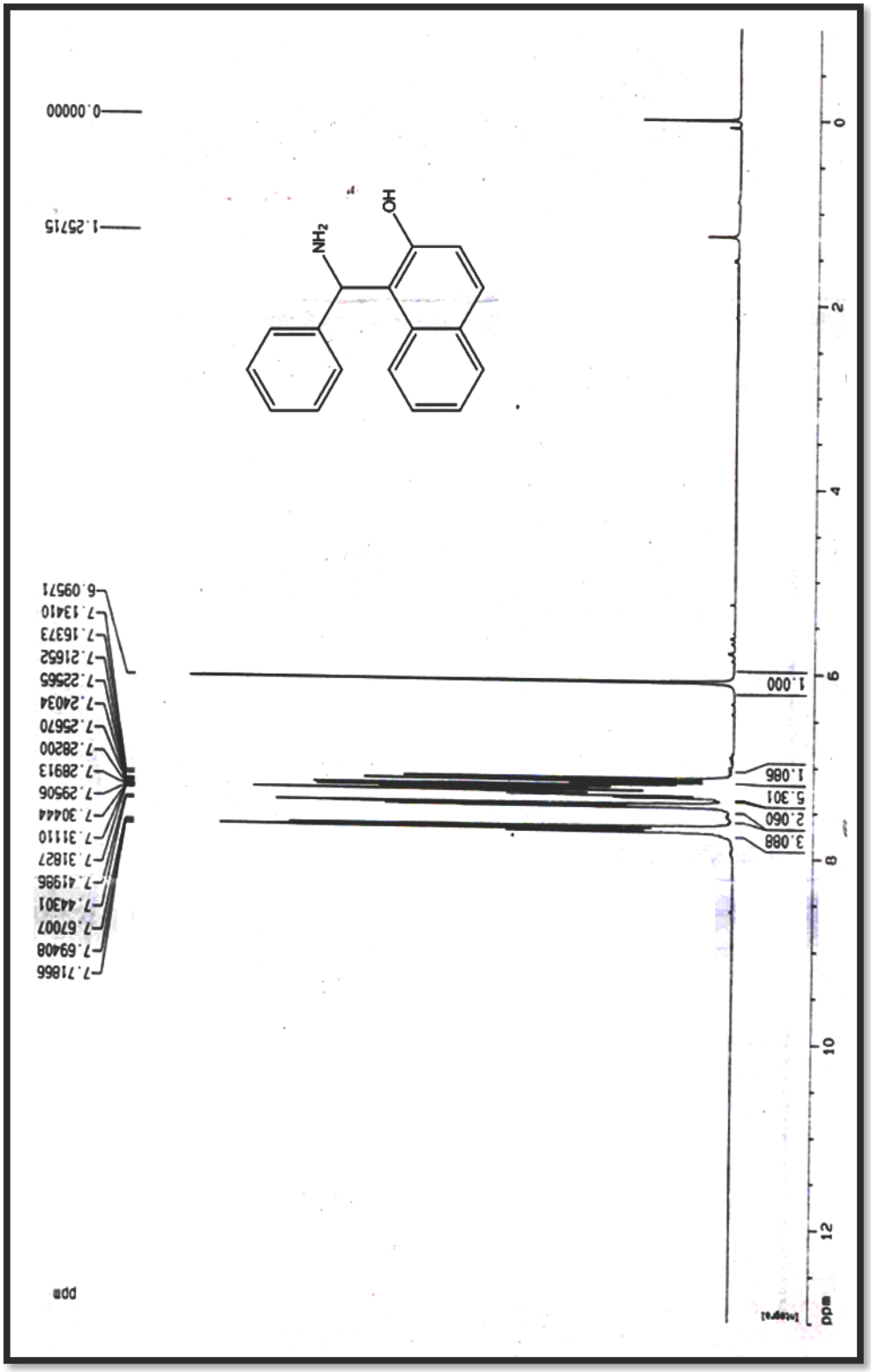

2.2SI ^{1}H NMR of BB

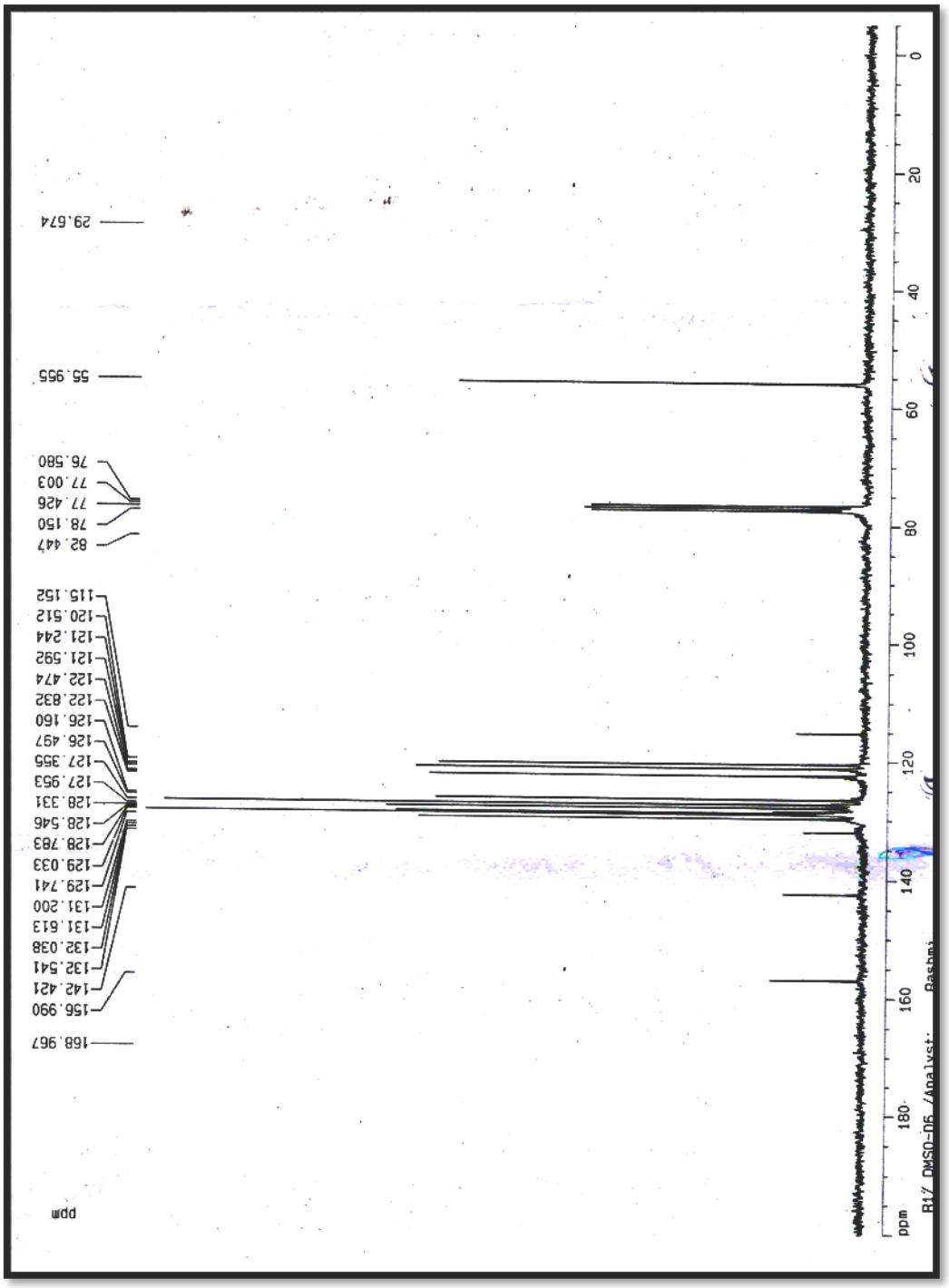

2.3SI ^{13}C NMR spectrum of BB

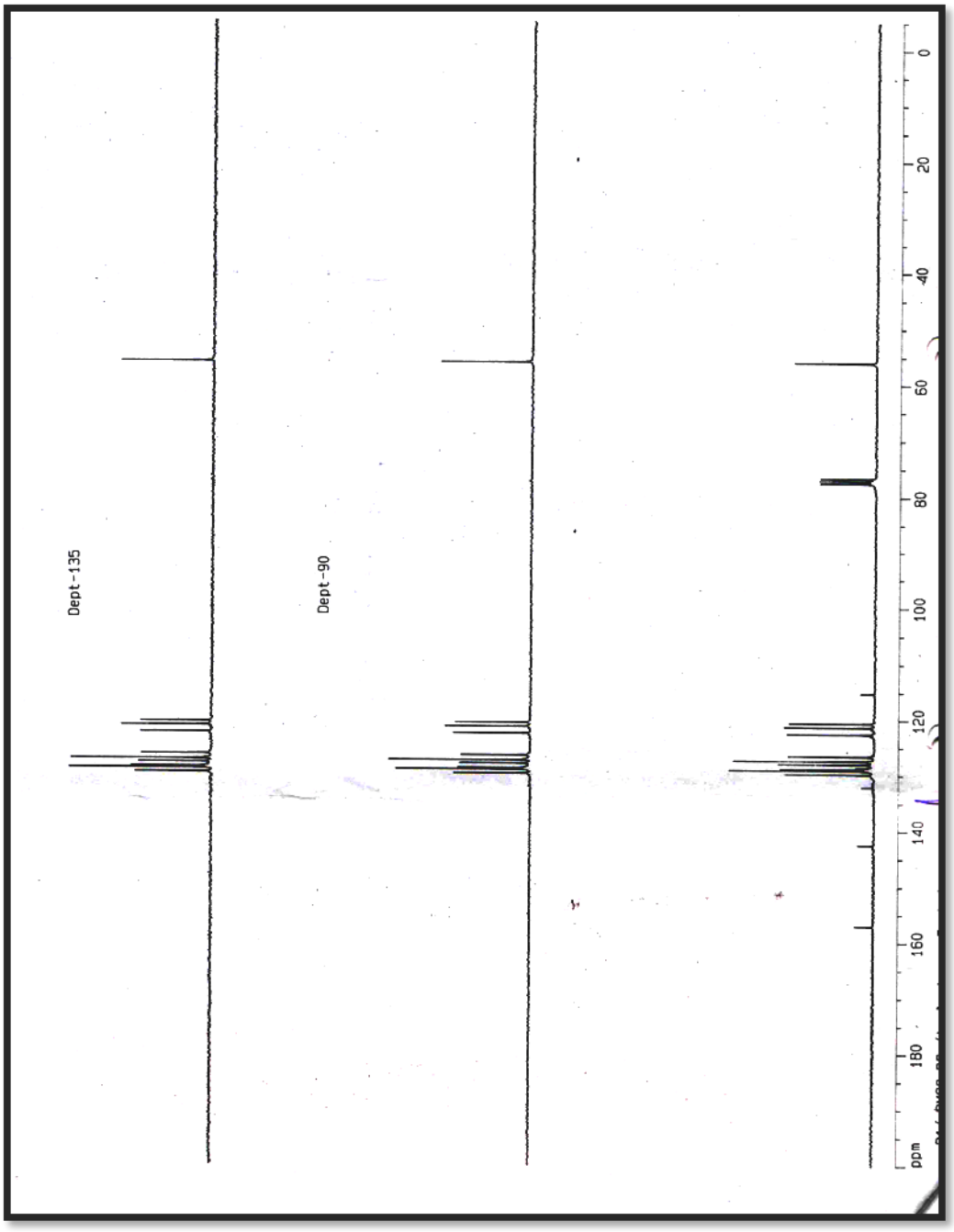

2.4SI DEPT analysis of BB

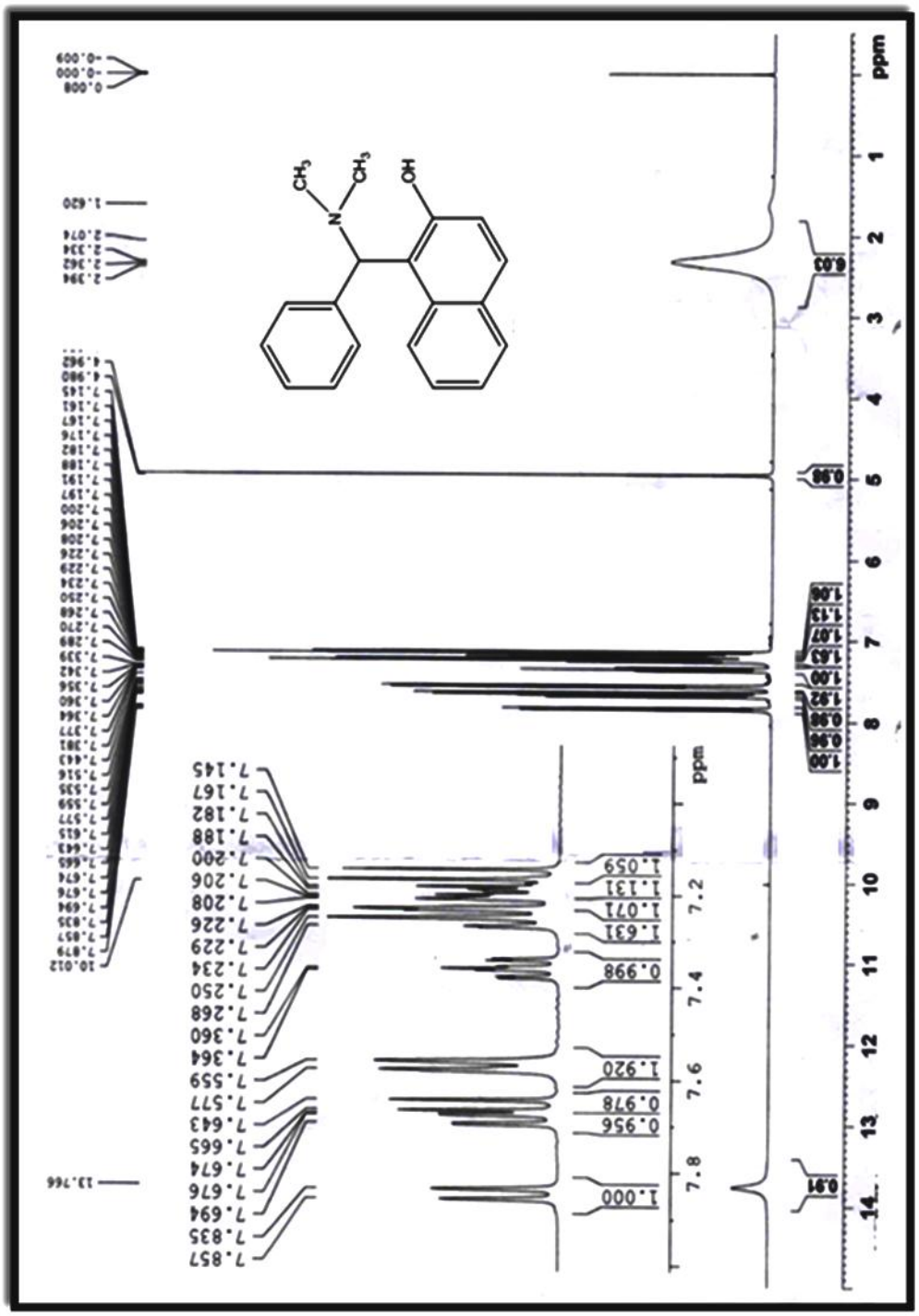

2.5SI ^{1}H NMR spectrum of DBB

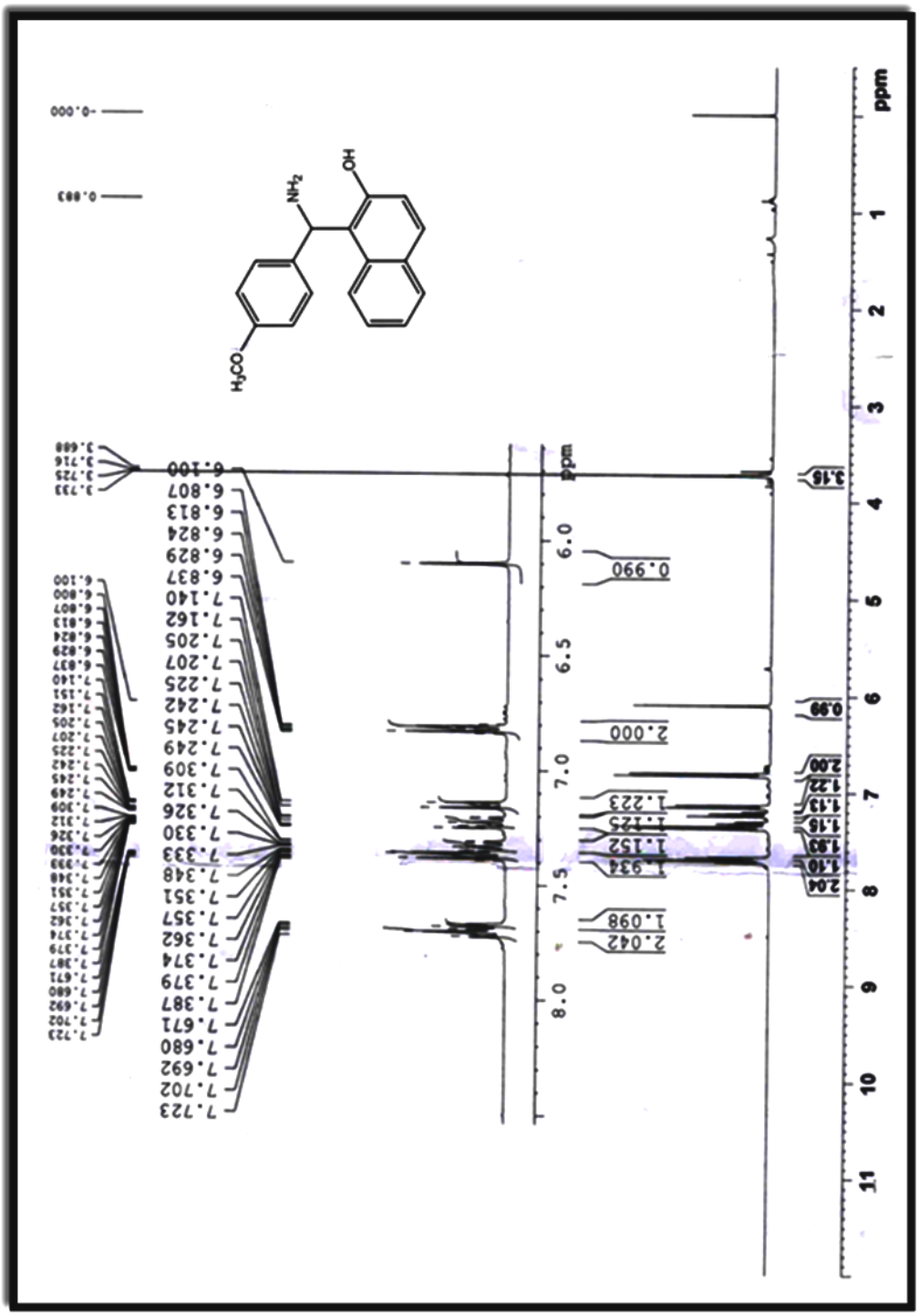

2.6SI ^{1}H NMR spectrum of ABB

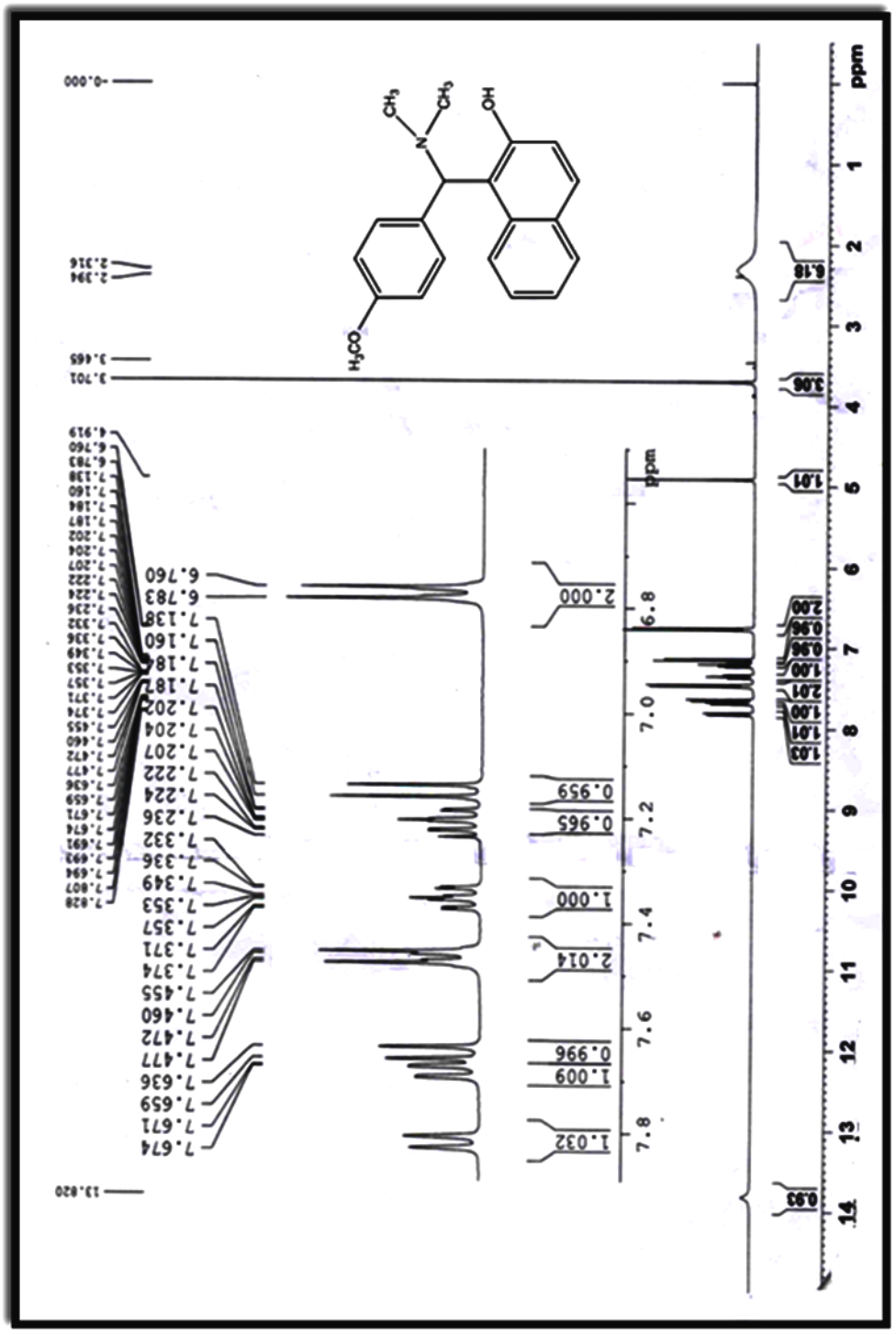

2.7SI ^{1}H NMR spectrum of ADBB

2.7. References

[1] a) S. Berlingozzi, *Gazz. Chim. Ital.* **1953**, 83, 693–719; b) G. Rosini, *Rendiconti Accademia Nazionale delle Scienze, Memorie di Scienze Fisiche Naturali* **2003**, 27, 1–35.

[2] M. Betti, *Gazz. Chim. Ital*. **1900**, 30 II, 310–316.

[3] H. E. Smith, N. E. Cooper, *J. Org. Chem.* **1970**, 35, 2212–2215.

[4] M. Betti, *Gazz. Chim. Ital*. **1906**, 36 II, 392–394.

[5] C. Cardellicchio, G. Ciccarella, F. Naso, E. Schingaro, F. Scordari, *Tetrahedron: Asymmetry*, **1998**, 9, 3667–3675.

[6] Y. Dong, R. Li, J. Lu, X. Xu, X. Wang, Y. Hu, *J. Org. Chem.* **2005**, 70, 8617–8620.

[7] V.A. Alfonsov, K.E. Metlushka, C.E. Mc Kenna, B.A. Kashgemirov, O.N. Kataeva, V.F. Zheltukhin, D.N. Sadkova, A.B. Dobrynin, *Synlett* **2007**, 488–490.

[8] J.B. Littman, W.R. Brode, *J. Am. Chem. Soc*. **1930**, 52, 1655–1659.

[9] M. Periasamy, M.N. Reddy, S. Anwar, *Tetrahedron: Asymmetry* **2004**, 15, 1809–1812.

[10] I. Szatmari, T.A. Martinek, L. Lazar, F. Fulop, *Tetrahedron* **2003**, 59, 2877–2884.

[11] I. Szatmari, T.A. Martinek, L. Lazar, A. Koch, E. Kleinpeter, K. Neuvonen, F. Fulop, *J. Org. Chem.* **2004**, 69, 3645–3653.

[12] D. Toth, I. Szatmari, F. Fulop, *Eur. J. Org. Chem.* **2006**, 69, 4664–4669.

[13] R.G. Xiong, *Lett. Org. Chem.* **2008**, 5, 265–268.

[14] P.D. MacLeod, Z. Li, J. Feng, C.J. Li, *Tetrahedron Lett*. **2006**, 47, 6791–6794.

[15] G. Palmieri, *Tetrahedron: Asymmetry* **2000**, 11, 3361–3373.

[16] C. Cimarelli, A. Mazzanti, G. Palmieri, E. Volpini, *J. Org. Chem*. **2001**, 66, 4759–4765.

[17] C. Cimarelli, G. Palmieri, E. Volpini, *Tetrahedron: Asymmetry* **2002**, 13, 2417–2426.

[18] J.X. Ji, L.Q. Qiu, C.W. Yip, A.S.C. Chan, *J. Org. Chem.* **2003**, 68, 1589–1590.

[19] J.X. Ji, J. Wu, T.T.L. Au-Teung, C.W. Yip, R.K. Haynes, A.S.C. Chan, *J. Org. Chem.* **2005**, 70, 1093–1095.

[20] I. Szatmari, F. Fulop, *Synthesis* **2009**, 775–778.

[21] M. Ghandi, A. Olyaei, S. Raoufmoghaddam, *Synthetic Communications* **2008**, 38, 4125–4138.

[22] A. Kumar, M.K. Gupta, M. Kumar, *Tetrahedron Letters* **2010**, 51, 1582–1584.

[23] a) T. Maki; Y. Araki; Y. Ishida; O. Onomura; Y. Matsumura, *J. Am.Chem. Soc.* **2001**, *123*, 3371–3372; b) F. Thomas, O. Jarjayes, H. Jamet, S. Hamman, E.S. Aman, C. Duboc, J. L. Pierre, Angew. Chem. Int. Ed., 2004, 43, 594–597.

[24] C. Costentin, M. Robert, J.M. Saveant, *Chem. Rev.* **2010,** *110,* PR1–PR40.

[25] C. Costentin, M. Robert, J.M. Saveant, *J. Am. Chem. Soc.* **2006**, 128, 4552–4553.

[26] I.J. Rhile, T.F. Markle, H. Nagao, A.G. DiPasquale, O.P. Lam, M.A. Lockwood, K. Rotter, J.M. Mayer, *J. Am. Chem. Soc***. 2006**, 128, 6075–6088.

[27] I.J. Rhile, J.M. Mayer, *J. Am. Chem. Soc***. 2004**, 126, 12718–12719.

[28] T.F. Markle, J.M. mayer, *Angew. Chem. Int. Ed*. **2008**, 47, 738 –740.

[29] J.J. Warren, T.A. Tronic, J.M. Mayer, *Chem. Rev.* **2010,** 110, 6961–7001.

[30] M.V. Huynh, T.J. Meyer, *Chem. Rev*. **2007,** 107, 5004–5064.

[31] J.M. Mayer, I.J. Rhile, *Biochimica et Biophysica Acta* **2004**, 1655, 51– 58.

[32] C. Costentin, M. Robert, J.M. Saveant, *Phys. Chem. Chem. Phys.* **2010**, 12, 11179–11190.

[33] C. Costentin, C. Louault, M. Robert, J.M. Saveant, *PNAS* **2009**, 106, 18143–18148.

[34] J.M. Saveant, *Annu. Rev. Anal. Chem.* **2014**, 7, 537–560.

[35] J.M. Saveant, C. Tard, *J. Am. Chem. Soc*. **2014**, 136, 8907−8910.

[36] C. Costentin, M. Robert, J.M. Saveant, C. Tard, *Acc. Chem. Res.* **2014**, 47, 271–280.

[37] J.N. Schrauben, M. Cattaneo, T.C. Day, A.L. Tenderholt, J.M. Mayer, *J. Am. Chem. Soc.* **2012**, 134, 16635−16645.

[38] T.F. Markle, I.J. Rhile, A.G. DiPasquale, J.M. Mayer, *PNAS* **2008**, 105, 8185–8190.

[39] J.L. Dempsey, J.R. Winkler, H.B. Gray, *Chem Rev*. **2010**, 110, 7024–7039.

[40] J. Bonin, C. Costentin, M. Robert, J.M. Saveant, *Org. Biomol. Chem.* **2011**, 9, 4064–4069.

[41] a) G. Pandey, S. Pal, R. Laha, *Angew. Chem.* **2013**, 125, 5250–5253; *Angew. Chem. Int. Ed*. **2013**, 52, 5146–5149; b) C.J. Li, *Acc. Chem. Res*. **2009**, 42, 335–

344; c) P. Xie, Y. Xie, B. Qian, H. Zhou, C. Xia, H. Huang, *J. Am. Chem. Soc.* **2012**, 134 9902–9905; d) Z. Li, Li. Cao, C.-J. Li, *Angew. Chem.* **2007**, 119, 6625–6627; *Angew. Chem. Int. Ed.* **2007**, 46, 6505–6507; e) Z. Li, C. J. Li, *J. Am. Chem. Soc.* **2005**, 127, 3672–3673.

[42] a) S.J. Park, J.R. Price, M.H. Todd, *J. Org. Chem.* **2012**, 77, 949–955; b) L. Liu, P. E. Floreancig, *Angew. Chem.* **2010**, 122, 6030–6033; *Angew. Chem. Int. Ed*. **2010**, 49, 5894–5897; c) B. Yu, T. Jiang, Y. Su, X. Pan, X. She, *Org. Lett.* **2009**, 11, 3442–3445; d) Y. Zhang, C. J. Li, *J. Am. Chem. Soc.* **2006**, 128, 4242–4243.

[43] A. J. Bard and L. R. Faulkner, *Electrochemical Methods, Fundamentals and Applications*, John Wiley & Sons, New York, NY, USA, 1980.

[44] O. Draˇcka, *Journal of Electroanalytical Chemistry*, **1996**, 402, 19–28.

[45] L. Trnkov´a, O. Draˇcka, *Journal of ElectroanalyticalChemistry*, **1996**, 413, 123–129.

[46] N. Serrano, A. Alberich, L. Trnkova, *Electroanalysis*, **2012**, 24, 955–960.

[47] L. Trnkova, L. Zerzankova, F. Dycka, R. Mikelova, F. Jelen, *Sensors*, **2008**, 8, 429–444.

[48] M. ˇSupicov´a, R. Rozik, L. Trnkov´a, R. Oriˇn´akov´a, M. G´alov´a, *Journal of Solid State Electrochemistry*, **2006**, 10, 61–68.

[49] L. Trnkov´a, I. Postbieglov´a, M.Holik, *Bioelectrochemistry*, **2004**, 63, 25–30.

[50] L. Trnkov´a, *Talanta*, **2002**, 56, 887–894.

[51] L. Trnkova, R. Kizek, V. Adam, T. Eckschlager, and J. Hubalek, *Sensing in Electroanalysis*, vol. 5, University Press Centre, Pardubice, Czech Republic, 2010.

[52] L. Trnkov´a, F. Jelen, I. Postbieglov´a, *Electroanalysis*, **2006**, 18, 662–669.

[53] L. Trnkov´a, F. Jelen, I. Postbieglov´a, *Electroanalysis*, **2003**, 15, 1529–1535.

[54] L. Trnkova, F. Jelen, J. Petrlova, V. Adam, D. Potesil, R. Kizek, *Sensors*, **2005**, 5, 448–464,.

[55] L. Trnkov´a, *Journal of Electroanalytical Chemistry*, **2005**, 582, 258–266.

[56] *Matlab Version 7.3.0.267*, Mathworks Inc., Natick, Mass, USA, 2006.

[57] F. Jelen, A. Kourilova, S. Hason, R. Kizek, L. Trnkova, *Electroanalysis*, **2009**, 21, 439–444.

[58] N. Aladag, L. Trnkova, A. Kourilova, M. Ozsoz, F. Jelen, *Electroanalysis*, **2010**, 22, 1675–1681.